Electron Tunneling in Blue and Purple Copper Proteins

Thesis by

Kevin Richard Hoke

In Partial Fulfillment of the Requirements

for the Degree of

Doctor of Philosophy

California Institute of Technology

Pasadena, California

2002

(Defended August 10, 2001)

Acknowledgements

There is a story of an emperor who commissioned an artist to make a simple painting of a rooster. Days and weeks passed and the emperor sent squires and stewards to check on the painter's progress, but despite the emperor's growing impatience, the work was not finished. As weeks turned into months and then into years, the emperor himself went to the painter and demanded to see the painting. The artist then took a blank canvas and with quick, brilliant strokes painted a perfect representation of a rooster. The emperor was stunned at the beauty of the work, but then became enraged: "If that is all the time that was needed, then why have you kept me waiting so long? Tell me why I should not have you put to death for this insolence!" The artist said nothing, but drew back a curtain revealing a room with stacks and stacks of countless canvases bearing lesser renditions of the rooster.

Fortunately, some thesis advisors are more patient than the enraged emperor above, who most likely put the artist to death anyway since enraged petty tyrants seldom appreciate subtle messages, and to be realistic, this is just a drawing of a rooster, not the Sistine Chapel. Therefore, first and foremost I am grateful to Harry Gray – no other advisor could have been as supportive and as patient as he has been with me and no words here can repay him for that.

Furthermore, in my time in the Gray Group I have had the honor and privilege to work with more people than I can readily name. Dr. Angelo Di Bilio was exceedingly generous with his time, expertise, and patience, all of which made this work possible. I am also grateful to Prof. Jack Richards and Dr. Cynthia Kiser for our collaborative efforts with purple copper. I thank Dr. Jay Winkler and Randy Villahermosa for assistance in BILRC, Prof. Mike Hill for discussions of matters electrochemical, and Dr. Michele McGuirl for patience above and beyond the call of duty in guiding me through applied molecular biology.

To all of the Gray group, from Don and Kara to Will and Julia and all those in between, I give my gratitude for keeping things lively. También, muchas gracias a Cindy y la familia Quezada por todo. Finally, I would like to thank my family, especially my parents, who never let on that I said "just another couple of years" more than once.

Abstract

The Cu_A domain is the initial point of entry for electrons into cytochrome *c* oxidase. In order to explain fast rates of intramolecular electron transfer (ET) over long distances, it has been suggested that the ET reorganization energy is less than 0.6 eV. This issue was investigated by attaching a ruthenium(II)-bisbipyridyl-imidazole complex to a single surface histidine of the *Thermus thermophilus* Cu_A domain. Photoexcitation results in rapid ET between the ruthenium complex and the copper site. This was done over a range of driving forces by employing a series of substituted bipyridines. An analysis of the driving force dependence of the ET rate suggests that the total reorganization energy for this Cu_A fragment is about 0.7 eV, almost as high as for azurin. The degree of solvent exposure of the active site may be the factor responsible for the higher reorganization energy.

In addition, the effect of distance on ET rate was investigated. Two variants of ruthenium-modified Cu_A were examined, in which the labeled sites are two positions apart. The observed ET rates only differ by an order of magnitude, drastically less than what theory would predict. It appears that geometric factors other than length influence ET coupled through hydrogen bonds.

The role of hydrogen bonds in ET was studied in more detail with ruthenium-modified azurin. Changes in the ET rate were observed for different degrees of deuterium incorporation in the system. For wild-type azurin, the greatest effect ($k_H/k_D \approx 0.7$) is seen when the protein is subjected to rigorous exchange under denaturing conditions, then returned to a normal buffer as a control for the solvent isotope effect on the reorganization energy. This is the expected outcome if deuteration of internal, difficult to exchange hydrogen bonds results in improved coupling along the path.

Table of Contents

List of Tables and Figures

Chapter 2

Chapter 3

Chapter 4

Chapter 1

Overview of Thesis

ET reorganization energy in Cu_A

In Chapter 2, the reorganization energy for electron transfer (ET) in a water-soluble Cu_A domain is determined. It has been suggested that the ET reorganization energy for Cu_A is less than 0.6 eV.[1] In order to examine this matter, a ruthenium(II)-bisbipyridyl-imidazole complex was attached to a single surface histidine at position 117 (wild type) or 119 (mutant) on the polypeptide chain of the *Thermus thermophilus* Cu_A domain. Photoexcitation of $RuCu_A$ resulted in rapid reduction of the dicopper site to Cu^+Cu^+. The rates of conversion of the transient Cu^+Cu^+–Ru^{3+} species back to Cu^+Cu^{2+}–Ru^{2+} were measured by time-resolved absorption spectroscopy for both modified proteins.

This was done over a range of driving forces by employing a series of substituted bipyridines. An analysis of the driving force dependence of the ET rate using semiclassical ET theory shows that the total reorganization energy, λ, for this Cu_A fragment is nearly as high as that of azurin ($\lambda \approx 0.8$ eV).[2] Comparison to another Cu_A system[3] suggests that the degree of solvent exposure of the active site may influence the value of λ.

ET pathways in Cu_A

In Chapter 3, it is shown that for two variants of $RuCu_A$, in which the labeled positions are two residues removed from one another, the observed ET rate only differs by an order of magnitude. This is significantly less than what the relative donor-acceptor distances would suggest.[4] Analysis in terms of the pathways model[5] is more successful in explaining the discrepancy, once consideration is given to the geometry of the hydrogen bonds in the appropriate pathways. Implications of the pathways model for ET from Cu_A to heme *b* in the intact oxidase from *T. thermophilus* are also discussed.

Role of hydrogen bonds in ET in azurin

Chapter 4 discusses electron transfer between the blue copper site of azurin and ruthenium(II)-bisbipyridyl-imidazole complexes attached to histidine side chains on the protein surface. The importance of hydrogen bonds in mediating intramolecular ET is addressed by examining deuterium isotope effects. Changes in the ET rate were observed for different degrees of deuterium incorporation in the system, suggesting that changes in hydrogen bond properties can affect the ET rate. While a normal isotope effect is seen for simple buffer exchange ($k_H/k_D \approx 1.6$), an inverse isotope effect ($k_H/k_D \approx 0.7$) is seen when the protein is subjected to rigorous exchange under denaturing conditions, then returned to a normal buffer as a control for the solvent isotope effect on the reorganization energy. This outcome differs somewhat from the result of a similar experiment,[6] probably due to the complex interplay of multiple isotope dependences.

References

(1) Larsson, S.; Källebring, B.; Wittung, P.; Malmström, B. G. *Proc. Natl. Acad. Sci. U. S. A.* **1995,** *92*, 7167-7171.

(2) Di Bilio, A. J.; Hill, M. G.; Bonander, N.; Karlsson, B. G.; Villahermosa, R. M.; Malmstrom, B. G.; Winkler, J. R.; Gray, H. B. *J. Am. Chem. Soc.* **1997**, *119*, 9921-9922.

(3) Hay, M.; Richards, J. H.; Lu, Y. *Proc. Natl. Acad. Sci. U. S. A.* **1996**, *93*, 461-464.

(4) Moser, C. C.; Page, C. C.; Chen, X.; Dutton, P. L. *J. Biol. Inorg. Chem.* **1997**, *2*, 393-398.

(5) Beratan, D. N.; Onuchic, J. In *Protein Electron Transfer*; Bendall, D. S., Ed.; BIOS Scientific Publishers Ltd.: Oxford, 1996; pp 23-42.

(6) Farver, O.; Zhang, J. D.; Chi, Q. J.; Pecht, I.; Ulstrup, J. *Proc. Natl. Acad. Sci. U. S. A.* **2001**, *98*, 4426-4430.

Chapter 2

Reorganization Energy in the Soluble Cu_A Domain from *Thermus thermophilus*

Introduction

The copper A (Cu_A) domain is the initial point of entry for electrons into cytochrome *c* oxidase (Figure 2.1), the enzyme that catalyzes the four-electron reduction of oxygen to water with the concomitant transport of protons across the inner membrane in bacteria and mitochondria.[1] This is a critical component of the respiratory cycle, eventually leading to the storage of chemical energy in the form of ATP. The four necessary electrons are brought into the system one at a time by the small electron transport protein, cytochrome *c*, which binds at the Cu_A domain.[2,3]

The binuclear Cu_A site (Figure 2.2) exhibits a reversible one-electron redox couple[4] in which the unpaired electron in the oxidized "Cu^{2+}/Cu^{+}" form is delocalized over both coppers.[5-7] After each one-electron reduction of Cu_A, rapid electron transfer (ET) occurs over a distance of about 20 Å from Cu_A to heme *a*/*b*.[8-11] The driving force for this reaction is only 50 mV,[12] suggesting that the total reorganization energy, λ, is less than 0.6 eV.[13-15] This value is somewhat less than that seen for the blue copper proteins, such as azurin (λ = 0.8 eV).[16]

The Cu_A domain is primarily a beta-fold structure,[17,18] as is the case for the single copper ET proteins. There are two postulations as to why this cupredoxin domain has an additional copper in the active site.[13] First, a dicopper center would better direct the unidirectional electron flow through the domain from the cytochrome *c* docking site to the interface with Subunit II, in which the catalytic center is located (Figure 2.1). On the other hand, the soluble blue copper proteins are free to dissociate between their redox partners and use the same docking site for both.

The second explanation involves the delocalized electronic structure of the dicopper site. For small changes in geometry, an approximation can be used to predict the effect on the inner sphere reorganization energy, λ_i:[14]

$$\lambda_i \approx kn(\Delta r)^2, \text{ where}$$

k is the effective force constant for distortion

n is the number of metal ligand bonds in the inner sphere and

Δr is the average change in bond length.

Accordingly, the tetrahedral core in the Cu_A center may compensate for the increased number of inner sphere atoms with smaller changes in bond lengths and lower vibrational energies. Furthermore, the electronic delocalization over this core increases the effective charge radius, leading to a reduction in the outer sphere reorganization energy.[19] Thus, the burden of the one-electron redox process is "shared" by both coppers and can be accommodated with less total reorganization.

In this chapter, the reorganization energy for ET in a water-soluble Cu_A domain is investigated through spectroscopic observations of photoinduced intramolecular ET. A ruthenium(II)-bisbipyridyl-imidazole complex is attached to a single surface histidine at position 119 (i.e., in a H117Q/E119H mutant) of the *Thermus thermophilus* Cu_A domain. (Figure 2.3) Photoexcitation triggers ET events that are observed by time-resolved absorption spectroscopy. This is done over a range of driving forces by employing a series of ruthenium labels of differing potential. An analysis of the results using semiclassical ET theory suggests that the total reorganization energy for this Cu_A fragment is not much lower than that of azurin.

Materials and Methods

General

The expression and purification of the Cu_A subdomain from *T. thermophilus* are described in Appendix A, with early efforts assisted by Dr. Cynthia Kiser.[20,21] Protein mass spectrometry was performed by the Caltech Protein/Peptide Microanalytical Laboratory. Some electrochemical measurements were made with the assistance of Prof. Michael Hill at Occidental College. UV-Visible absorption spectra were obtained with a HP-8452 spectrophotometer. Ruthenium complexes other than bis(4,5,4',5'-tetramethyl-2,2'-bipyridine)dichloro ruthenium were obtained from existing stocks in the laboratory, prepared according to literature.[22,23]

Ruthenium complex labeling

The ruthenium complexes $Ru(bpy)_2CO_3$, $Ru(Me_2bpy)_2CO_3$, and $Ru(Me_4bpy)_2CO_3$ were used to label $His119Cu_A$, the H117Q/E119H mutant of Cu_A ("bpy" = 2,2'-bipyridine, "Me_2bpy" = 4,4'-dimethylbpy, and "Me_4bpy" = 4,5,4',5'-tetramethylbpy). Me_4bpy was prepared from the reflux of 3,4-lutidine over 5% Pd/C, followed by extraction into ethyl acetate.[24] Several procedures for the synthesis of $Ru(Me_4bpy)_2Cl_2$ were attempted[23,25] but the most satisfactory results were obtained from that of Gould, et al.[26] The chloride complex was converted to the carbonate for improved reactivity.[22]

$His119Cu_A$ at 200-300 μM was incubated with 1.2 equivalents of the ruthenium complex in 300 mM sodium bicarbonate, pH = 8.3. The ruthenium complex was best dissolved in 30% methanol and added in aliquots over 48 hours, during which time the reaction was kept in the dark at room temperature. The Me_4bpy complex was much less

soluble and more prone to oxidation than the bpy and Me_2bpy complexes were. In that case, it was necessary keep the reaction under argon, and the ruthenium complex was added in one portion. In addition, a magnetic stir bar was used to prevent settling of the ruthenium complex at the bottom of the reaction vessel. The total incubation time required for reaction was varied according to the reactivity of both the histidine position and the ruthenium complex.

After the reaction was judged complete, the vessel was opened and the excess ruthenium complex was washed away using a Centricon-10 (Millipore), or else passed down a PD-10 gel filtration column prepacked with G-25 Sephadex (Pharmacia). This also accomplished the exchange into 20 mM HEPES w/ 750 mM NaCl, pH = 7. The protein was allowed to equilibrate with this buffer overnight at 5°C to promote dissociation of any ionically bound ruthenium complex.

Labeled and unlabeled forms of the protein were separated using FPLC with a 10/2 Chelating Sepharose column (Pharmacia) charged with copper sulfate and equilibrated with 20mM HEPES containing 750 mM NaCl. Elution was performed using a gradient with a second buffer containing 750 mM NH_4Cl rather than NaCl. Fractions were evaluated by optical spectroscopy according to the position of the peak near 496 nm and its intensity compared to that of the Cu_A band at 790 nm. The first peaks from the column were the multiply labeled forms of the protein, distinctly orange in color, then came the singly labeled forms, more pink in appearance, and finally, the unlabeled protein. The free *N*-terminus form of the labeled protein had greater affinity for the column than did the *N*-acetyl form, whose elution often overlapped with the multiply labeled forms. The exception was the R146H mutant, which had less affinity for this column than the other two varieties studied. When

necessary, further purification was carried out using Mono Q anion exchange chromatography (Appendix A).

The singly labeled protein was then equilibrated into potassium phosphate buffer (μ = 0.1, pH = 7). Following characterization by mass spectrometry and UV-Vis spectroscopy, the sample is reduced to about 1 mL in volume and mixed with an equal volume of 200 μM imidazole•HCl, pH = 7.5. The sample was degassed by repeated pump/fill cycles with argon and allowed to incubate in the dark until an orange fluorescence was visible under a UV lamp. During this incubation, the protein is susceptible to copper loss; therefore, excessive concentrations of imidazole or higher pH are to be avoided. Once the sample had attained a suitable level of imidazole incorporation, the excess could be removed by gel filtration (PD-10) or ultrafiltration (Centricon-10). The final product was kept at –5°C in the dark and used promptly for ET measurements.

Electrochemistry of Cu_A and ruthenium labeled forms

Electrochemical measurements were obtained using an edge plane graphite electrode, polished successively with 0.3 μm and 0.05 μm alumina, sonicated in water for 15 minutes, and dried with a heat gun. A three-arm cell, in which the sample chamber was separated from the platinum wire auxiliary electrode by a glass frit and from the Ag/AgCl reference electrode by a modified Luggin capillary, was used. The buffer used was potassium phosphate, μ = 0.1, pH = 7.

Kinetic measurements

Photoinduced electron transfer was studied by laser flash spectroscopy in the Beckman Institute Laser Resource Center, using a setup described elsewhere.[27] Samples were

placed in an anaerobic quartz cuvette fitted for use with a Schlenk line. The samples were degassed by multiple pump/fill cycles with argon, taking care not to bubble the protein solution. Single wavelength transient absorption spectroscopy was used to follow the direct intramolecular photoinduced reduction of the Cu_A center by the ruthenium label followed by the reoxidation of the copper site by the transiently formed ruthenium species (Figure 2.8). This process was monitored at 318 nm, 431 nm, 530 nm and 798 nm. It was useful to measure the luminescence decay rate at 670 nm and use this value in analyzing the transient absorbance data. Temperature was monitored by means of a thermocouple lead inserted between the cuvette and a water-jacketed cell holder connected to a circulating water bath. Acquired data sets were analyzed in terms of multiple exponential decays with deconvolution and curve fitting performed using non-linear least squares fitting software developed at Caltech by Dr. Jay Winkler.

Results and Discussion

Metal labeling of His119Cu_A

The yields for ruthenium-labeled His119Cu_A decreased with the potential of the ruthenium complex (Rubpy > $RuMe_2bpy$ > $RuMe_4bpy$). This is consistent with the methyl groups imparting additional electron density onto the ruthenium center, leading to diminished reactivity of the ruthenium center with respect to the nucleophilic histidine ligand. As a result, reaction times were increased to 7-10 days for the Me_4bpy derivative. Furthermore, the reactivity of the Me_4bpy complex was hindered by its relative insolubility in aqueous solutions, despite presolubilization in methanol.

Incubation with imidazole is used to place an additional nitrogen ligand on the ruthenium center in $Ru(bpy)_2(H_2O)HisCu_A$. This yields a complex with a longer excited state lifetime and higher redox potential. However, incubation with excess imidazole can lead to depletion of copper in the protein and complete loss of the absorption bands corresponding to the dicopper site. Mass spectrometry for copper-depleted Cu_A reveals the presence of only one copper atom in the protein. The lack of visible absorption in copper-depleted unlabeled protein suggests that this is reduced copper.

Furthermore, the reversal of the copper loss in Cu_A is quite difficult, for reasons not fully understood. It has been reported that the initial uptake of copper by a Cu_A center *in vitro* is dependent on the prior reduction of aqueous copper(II), even at the expense of forming a disulfide bond using cysteines from another equivalent of apo-Cu_A.[28] Indeed, the best results for reintroduction of copper were obtained in the presence of DTT as an exogenous reductant. However, this reversal was never fully complete and hence the concentration of imidazole used in the incubation was decreased to 100 mM, the pH lowered

to 7.3, and the reaction supplemented with 5 mM $CuSO_4$. The electronic absorption spectrum of the product is consistent with the superimposition of the Cu_A spectrum and a ruthenium model complex (Figure 2.6), although a loss of intensity at 798 nm in some samples indicates partial loss of copper.

Other metal complexes were attempted, but the results were disappointing. An osmium polypyridyl complex would be useful, providing a lower driving force for ET, but yields were too low for the reaction of $Os(bpy)_2CO_3$ or $Os(trpy)(bpy)(OH_2)$ with Cu_A. An attempt to conduct the reaction with $Os(III)(bpy)_2$, which might be able to react more readily using associative ligand substitution, was also unsuccessful. A complex with a higher redox potential, Ru[bis(*N*-diethylcarbamoyl)bpy]$_2Cl_2$, did provide suitable yields of labeled Cu_A; however, no suitable conditions were found to overcome its low reactivity with imidazole and at the same time maintain the copper site.

ET rates in Cu_A

Photoinduced intramolecular electron transfer in $RuCu_A$ was monitored by single wavelength transient absorption spectroscopy. Measurements were made at several wavelengths: 431 nm, 530 nm, and 800 nm (Figure 2.10). The first of these is located at the isobestic for the absorption of the excited state and ground state; as a result, it gives the best measure of Ru(III) formation and decay. The second represents a mixture of Cu_A and ruthenium absorption bands, and gives a large signal (Figure 2.7). Changes at 800 nm are primarily due to the oxidation state of the copper site. Agreement among the rates measured at each of these wavelengths is a strong indication that the oxidation and reduction processes for both the ruthenium and the Cu_A site occur at the same rate and are due to long range ET.

ET rates were obtained from the fit of the transients to multiple exponential decays. As expected, there is a fast rate that corresponds to the decay of the excited state. This fast rate can be obtained directly from the luminescence decay at 670 nm. However, there are additional processes present. Somewhat unexpectedly, the excited state decay is best fit to two exponentials. The additional decay is probably due to the aquo form of $RuCu_A$, present in the sample when there is incomplete reaction with imidazole. Rather than risk depletion of copper in the sample by changing the conditions for the reaction with imidazole, the intramolecular ET rates were measured for the aquo forms of $RuCu_A$ and used to fit the ET kinetics in the samples containing a mixture of aquo and imidazole forms.

Intramolecular ET involving the aquo form of a ruthenium bis(bipyridyl)-labeled protein is not well understood. It has been observed in ruthenium-labeled amicyanin, plastocyanin, and HiPIP,[29] but is not observed in azurin. The production of charge-separated intermediate (i.e., Cu^+Cu^+–Ru^{3+}) is still quite fast ($>10^7$ s^{-1}), but the return rate is much slower. In $RuHis119Cu_A$ the slow phase is ≈ 60 s^{-1} (Figure 2.11), compared to ≈ 300 s^{-1} in plastocyanin. As determined from electrochemical measurements, the Ru(II/III) potential for $Ru(Me_2bpy)_2(H_2O)Cu_A$ is 600 mV, reducing the driving force for the ET reaction by about 340 mV compared to the imidazole form. Furthermore, this reaction probably involves a ruthenium(III)hydroxo intermediate, and hence a greater reorganization energy.

Reorganization energy of the Cu_A domain

The ET rates in $Ru(Me_nbpy)_2(im)His119Cu_A$, where n= 0, 2, 4 can be used to find a value for the total reorganization energy, λ_{TOT}, from the variation of rate with driving force ($-\Delta G°$). The driving force is determined from the difference in redox potentials for Cu_A and the relevant $Ru(Me_nbpy)_2(im)_2$ model complexes. The driving force is further adjusted by

+80 mV to compensate for the observed shifts in the ruthenium potential upon binding to a protein.[16,24] The best fit to the semiclassical ET rate relationship (Figure 2.12) gives values of $\lambda_{TOT} = 0.73(5)$ eV and $H_{AB} = 0.028(3)$ cm^{-1}, with errors estimated from comparable fits to subsets of the three points. The total reorganization energy represents an average of the values for each partner in the ET event; i.e., $\lambda(RuCu_A) = [\lambda(Cu_A) + \lambda(Ru)]/2$. Using $\lambda(Ru) = 0.78$,[30] one obtains $\lambda(Cu_A) = 0.7(1)$ eV. However, an interpretation that incorporates the low lying vibrational states of the Cu_A center would lead to some flattening of the rates in the inverted region.[31,32] This would give a result more consistent with a lower value for $\lambda(Cu_A)$.

Though the value of 0.7 eV is somewhat imprecise, it is greater than the various estimates for the Cu_A site in the intact oxidase ($\lambda < 0.3$ eV), [13,15,33,34] as well as the experimental value for that in purple Cu_A azurin (0.4 eV).[35] However, the relative amount of exposure of the Cu_A site to solvent may provide an explanation. The Cu_A site in the intact oxidase is located at the interface of subunits I and II, and is shielded from bulk solvent. The lower polarity of the protein matrix compared to water would be expected to reduce the outer sphere component of the reorganization energy (λ_o) significantly.[36] Therefore, the increase in the total reorganization energy for the soluble form of the Cu_A domain may result from an outer sphere effect, whereas the inner sphere component is probably very similar.

Similarly, that the reorganization energy is lower in purple Cu_A azurin than in the *T. thermophilus* fragment can be explained in terms of relative solvent exposure. A comparison of the crystal structures (Figure 2.13) reveals that the Cu_A site in purple Cu_A azurin is deeper in the protein interior and the surface exposed histidine is shielded somewhat by the side chains of the neighboring helix. On the other hand, the Cu_A site in the *T. thermophilus* fragment is closer to the surface, and the nitrogen of the histidine is more exposed.

In addition, the reduction potential is greater in purple Cu_A azurin ($E° = 283$ mV) [35] than in the *T. thermophilus* fragment (240 mV)[4] and the intact oxidase (260 - 280 mV).[12,37] While this may be related to the differences in solvent exposure, one of the consequences of greater electronic coupling within the Cu_2S_2 core is a higher reduction potential.[14] In addition, the shift in the transition found in the soluble domains and native Cu_A at 790 nm to 765 nm in purple Cu_A azurin may indicate greater delocalization. Another important difference is that the Cu-Cu distance in purple Cu_A azurin is shorter than that in the *T. thermophilus* form of Cu_A (2.4 vs. 2.5-2.6 Å)[18,38-40] and even with the removal of a histidine ligand by mutagenesis the site remains intact.[41] In fact, this removal of a histidine in purple Cu_A azurin leads to EPR and UV-Vis characteristics more like those of native Cu_A. It would appear that the inner sphere reorganization energy for purple Cu_A azurin is certainly lower than that for the soluble Cu_A domain and possibly lower than that for the Cu_A site in the intact oxidase.

Increased solvent exposure and reorganization energy

Solvent accessibility can also be correlated to the reduction potential. The soluble Cu_A domain *T. thermophilus* has a potential of 240 mV with reduction cell entropy, ΔS_{rc}, of –5.4 e.u.[4] The small magnitude of entropic change is consistent with a relatively small degree of nuclear motion and hence a low reorganization energy.[42] However, the potential of Cu_A in reduced bovine cytochrome *c* oxidase was found to be 280 mV at pH 7 with $\Delta S_{rc} = -33$ e.u.[37] Increasingly negative values for S_{rc} are likely due to an increase in order in the reduced state, possibly due to a tightening of the polypeptide support.[43] Taken together, these two results would seem to indicate that the reorganization energy for Cu_A in the fragment is less than that in the intact oxidase, despite the apparent difference in solvent exposure.

However, an increase in S_{rc} (i.e., less negative) for the blue copper proteins can also indicate greater solvent accessibility/reduced hydrophobicity of the active site, possibly due to solvent interactions with the nitrogen of the exposed histidine.[44,45] Similarly, a more positive enthalpic parameter for the reduction is also consistent with increased solvent exposure since the solvent dipoles can stabilize the oxidized form of the enzyme.[46] In fact, the enthalpic term for the Cu_A fragment from *T. thermophilus* is more positive than that for Cu_A of the intact oxidase (-11.9 *vs.* –21.5 kcal/mol).[4,37]

Conclusions

This work has found a value for the reorganization energy for the water-soluble Cu_A domain from *T. thermophilus* that is less than that of the single copper sites in the blue copper proteins, but higher than what has been predicted. However, this is consistent with other assessments, both theoretical and experimental, if one considers an increase in outer sphere reorganization energy due to the increased solvent exposure of the active site relative to the other systems. In general, greater solvent exposure is expected to increase the outer sphere reorganization energy, as the polarizability of the local environment increases. While the absolute magnitude of the entropic term for the reduction reaction may suggest less nuclear reorganization upon reduction, the exact relationship likely differs for a solvated small molecule relative to a buried redox center. An increase in solvent exposure for a metal site in a protein may correspond to a transition from a "buried" center to a "solvated" center, with a corresponding increase in reorganization energy and decrease in reduction potential.

References

(1) Malmström, B. G. In *Electron Transfer in Chemistry*; Balzani, V., Ed.; Wiley-VCH: Weinheim, Germany, 2001; Vol. 3, pp 39-55.

(2) Witt, H.; Malatesta, F.; Nicoletti, F.; Brunori, M.; Ludwig, B. *Eur. J. Biochem.* **1998**, *251*, 367-373.

(3) Lappalainen, P.; Watmough, N. J.; Greenwood, C.; Saraste, M. *Biochemistry* **1995**, *34*, 5824-5830.

(4) Immoos, C.; Hill, M. G.; Sanders, D.; Fee, J. A.; Slutter, C. E.; Richards, J. H.; Gray, H. B. *J. Biol. Inorg. Chem.* **1996**, *1*, 529-531.

(5) Slutter, C. E.; Gromov, I.; Epel, B.; Pecht, I.; Richards, J. H.; Goldfarb, D. *J. Am. Chem. Soc.* **2001**, *123*, 5325-5336.

(6) Fee, J. A.; Sanders, D.; Slutter, C. E.; Doan, P. E.; Aasa, R.; Karpefors, M.; Vänngård, T. *Bioch. Biophys. Res. Comm.* **1995**, *212*, 77-83.

(7) Bertini, I.; Bren, K. L.; Clemente, A.; Fee, J. A.; Gray, H. B.; Luchinat, C.; Malmstrom, B. G.; Richards, J. H.; Sanders, D.; Slutter, C. E. *J. Am. Chem. Soc.* **1996**, *118*, 11658-11659.

(8) Kobayashi, K.; Une, H.; Hayashi, K. *J. Biol. Chem.* **1989**, *264*, 7976-7980.

(9) Paula, S.; Sucheta, A.; Szundi, I.; Einarsdottir, O. *Biochemistry* **1999**, *38*, 3025-3033.

(10) Pan, L. P.; Hibdon, S.; Liu, R.-Q.; Durham, B.; Millett, F. *Biochemistry* **1993**, *32*, 8492-8498.

(11) Farver, O.; Einarsdóttir, Ó.; Pecht, I. *Eur. J. Biochem.* **2000**, *267*, 950-954.

(12) Moody, A. J.; Rich, P. R. *Biochim. Biophys. Acta* **1990**, *1015*, 205-215.

(13) Larsson, S.; Källebring, B.; Wittung, P.; Malmström, B. G. *Proc. Natl. Acad. Sci. U. S. A.* **1995**, *92*, 7167-7171.

(14) Gamelin, D. R.; Randall, D. W.; Hay, M. T.; Houser, R. P.; Mulder, T. C.; Canters, G. W.; de Vries, S.; Tolman, W. B.; Lu, Y.; Solomon, E. I. *J. Am. Chem. Soc.* **1998**, *120*, 5246-5263.

(15) Brzezinski, P. *Biochemistry* **1996**, *35*, 5611-5615.

(16) Di Bilio, A. J.; Hill, M. G.; Bonander, N.; Karlsson, B. G.; Villahermosa, R. M.; Malmstrom, B. G.; Winkler, J. R.; Gray, H. B. *J. Am. Chem. Soc.* **1997**, *119*, 9921-9922.

(17) Wittung, P.; Källebring, B.; Malmström, B. G. *FEBS Lett.* **1994**, *349*, 286-288.

(18) Williams, P. A.; Blackburn, N. J.; Sanders, D.; Bellamy, H.; Stura, E. A.; Fee, J. A.; McRee, D. E. *Nat. Struct. Biol.* **1999**, *6*, 509-516.

(19) Marcus, R. A.; Sutin, N. *Biochim. Biophys. Acta* **1985**, *811*, 265-322.

(20) Slutter, C. E.; Sanders, D.; Wittung, P.; Malmström, B. G.; Aasa, R.; Richards, J. H.; Gray, H. B.; Fee, J. A. *Biochemistry* **1996**, *35*, 3387-3395.

(21) Kiser, C. N. Thesis: "Biological Electron Transfer in Copper Proteins," California Institute of Technology, 1998.

(22) Johnson, E. C.; Sullivan, B. P.; Salmon, D. J.; Adeyemi, S. A.; Meyer, T. J. *Inorg. Chem.* **1978**, *17*, 2211-2215.

(23) Sullivan, B. P.; Salmon, D. J.; Meyer, T. J. *Inorg. Chem.* **1978**, *17*, 3334-3341.

(24) Mines, G. A. Thesis: "Cytochrome *c*: Folding Triggered by Electron Transfer. Rates of Heme Oxidation and Reduction at High Driving Forces," California Institute of Technology, 1997.

(25) Togano, T.; Nagao, N.; Tsuchida, H. K.; Hisamatsu, K.; Howell, F. S.; Mukaida, M. *Inorg. Chem. Acta* **1992**, *195*, 221-225.

(26) Gould, S.; O'Toole, T. R.; Meyer, T. J. *J. Am. Chem. Soc.* **1990**, *112*, 9490-9496.

(27) Bjerrum, M. J.; Casimiro, D. R.; Chang, I. J.; Dibilio, A. J.; Gray, H. B.; Hill, M. G.; Langen, R.; Mines, G. A.; Skov, L. K.; Winkler, J. R.; Wuttke, D. S. *J. Bioenerg. Biomembr.* **1995**, *27*, 295-302.

(28) Wang, X. T.; Ang, M. C.; Lu, Y. *J. Am. Chem. Soc.* **1999**, *121*, 2947-2948.

(29) Di Bilio, A. J., unpublished results.

(30) Mines, G. A.; Bjerrum, M. J.; Hill, M. G.; Casimiro, D. R.; Chang, I.-J.; Winkler, J. R.; Gray, H. B. *J. Am. Chem. Soc.* **1996**, *118*, 1961-1965.

(31) Daizadeh, I. *Proc. Natl. Acad. Sci. USA* **1997**, *94*, 3703-3708.

(32) Lee, E.; Medvedev, E. S.; Stuchebrukhov, A. A. *J. Chem. Phys.* **2000**, *112*, 9015-9024.

(33) Ramirez, B. E.; Malmström, B. G.; Winkler, J. R.; Gray, H. B. *Proc. Natl. Acad. Sci. U. S. A.* **1995**, *92*, 11949-11951.

(34) Sigfridsson, E.; Olsson, M. H. M.; Ryde, U. *J. Phys. Chem. B* **2001**, *105*, 5546-5552.

(35) Farver, O.; Lu, Y.; Ang, M. C.; Pecht, I. *Proc. Natl. Acad. Sci. U. S. A.* **1999**, *96*, 899-902.

(36) Marcus, R. A. *J. Chem. Phys.* **1956**, *24*, 979-989.

(37) Wang, H.; Blair, D. F.; Ellis, W. R.; Gray, H. B.; Chan, S. I. *Biochemistry* **1986**, *25*, 167-171.

(38) Robinson, H.; Ang, M. C.; Gao, Y.-G.; Hay, M. T.; Lu, Y.; Wang, A. H.-J. *Biochemistry* **1999**, *38*, 5677-5683.

(39) Blackburn, N. J.; de Vries, S.; Barr, M. E.; Houser, R. P.; Tolman, W. B.; Sanders, D.; Fee, J. A. *J. Am. Chem. Soc.* **1997**, *119*, 6135-6143.

(40) Hay, M. T.; Ang, M. C.; Gamelin, D. R.; Solomon, E. I.; Antholine, W. E.; Ralle, M.; Blackburn, N. J.; Massey, P. D.; Wang, X. T.; Kwon, A. H.; Lu, Y. *Inorg. Chem.* **1998**, *37*, 191-198.

(41) Wang, X. T.; Berry, S. M.; Xia, Y.; Lu, Y. *J. Am. Chem. Soc.* **1999**, *121*, 7449-7450.

(42) Sutin, N.; Weaver, M. J.; Yee, E. *Inorg. Chem.* **1980**, *19*, 1096-1097.

(43) Taniguchi, V.; Sailasuta-Scott, N.; Anson, F. C.; Gray, H. B. *Pure App. Chem.* **1980**, *52*, 2275-2281.

(44) Battistuzzi, G.; Borsari, M.; Loschi, L.; Righi, F.; Sola, M. *J. Am. Chem. Soc.* **1999**, *121*, 501-506.

(45) Sailasuta, N.; Anson, F. C.; Gray, H. B. *J. Am. Chem. Soc.* **1979**, *101*, 455-458.

(46) Battistuzzi, G.; Borsari, M.; Canters, G. W.; de Waal, E.; Loschi, L.; Warmerdam, G.; Sola, M. *Biochemistry* **2001**, *40*, 6707-6712.

Table 2.1. Rates at room temperature for photoinduced ET in $RuCu_A$

Complex	k_{ET} (s^{-1})	Driving Force (eV)	Corrected Driving Force (eV)
$Ru(bpy)_2(im)H119Cu_A$	2.28(2) x 10^5	0.84	0.84
$Ru(Me_2bpy)_2(im)H119Cu_A$	1.6(2) x 10^5	0.62[1]	0.70[2]
$Ru(Me_4bpy)_2(im)H119Cu_A$	3.3(3) x 10^5	0.56[1]	0.64[2]

[1] Determined from the difference in redox potentials for the corresponding $Ru(L)_2(im)_2$ model complex and Cu_A.

[2] Adjusted for +80 mV shift in observed Ru(II/III) potentials upon protein binding

Figure 2.1. The structure of cytochrome *c* oxidase from *T. thermophilus* (PDB 1EHK)

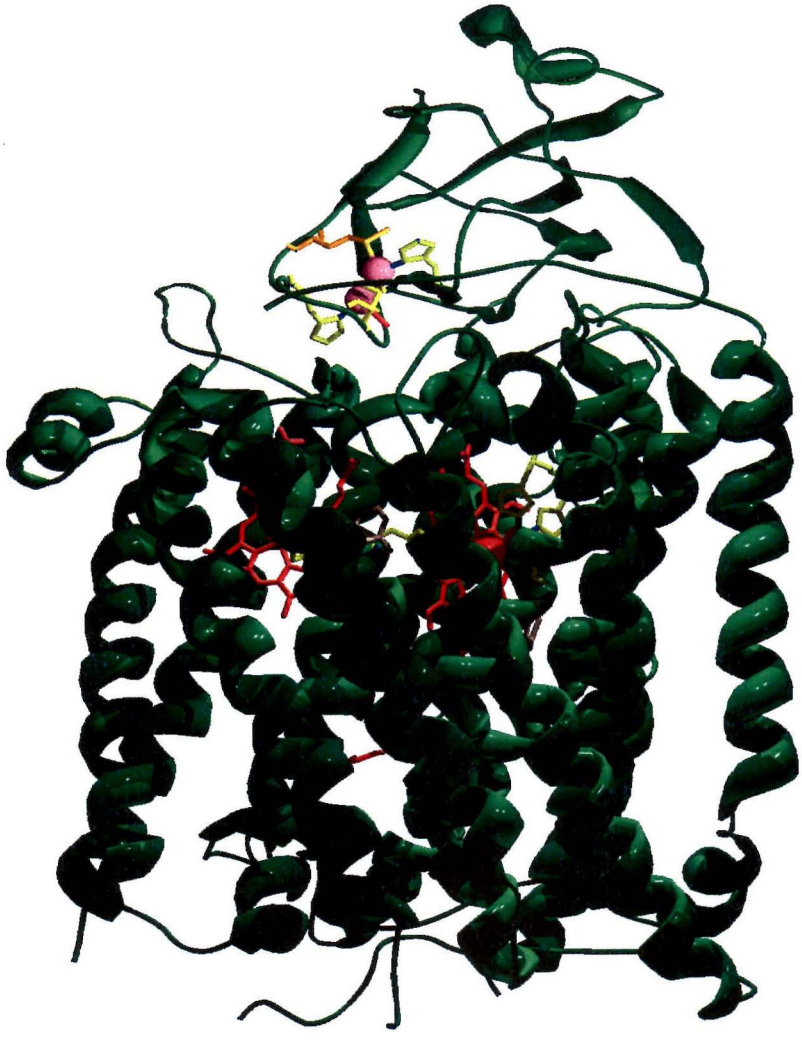

Figure 2.2. The Cu_A active site

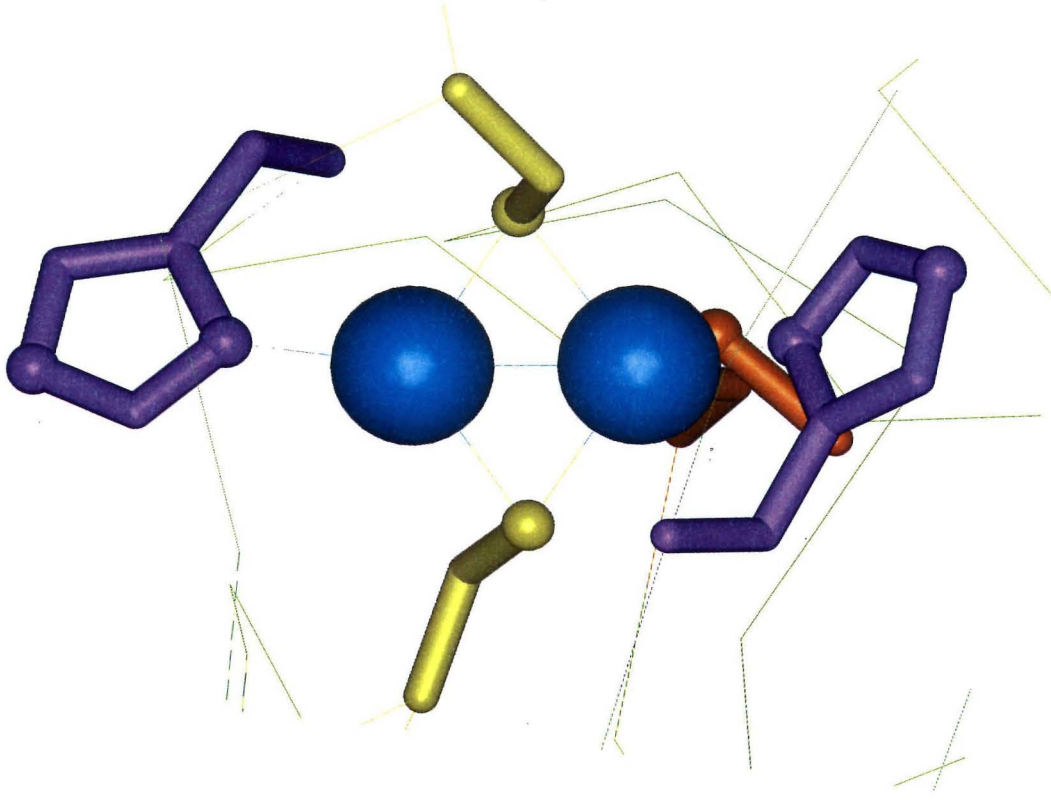

Figure 2.3. Ruthenium-modified Cu_A

The ruthenium complex was modeled using Insight II, taking care to minimize steric clashes.

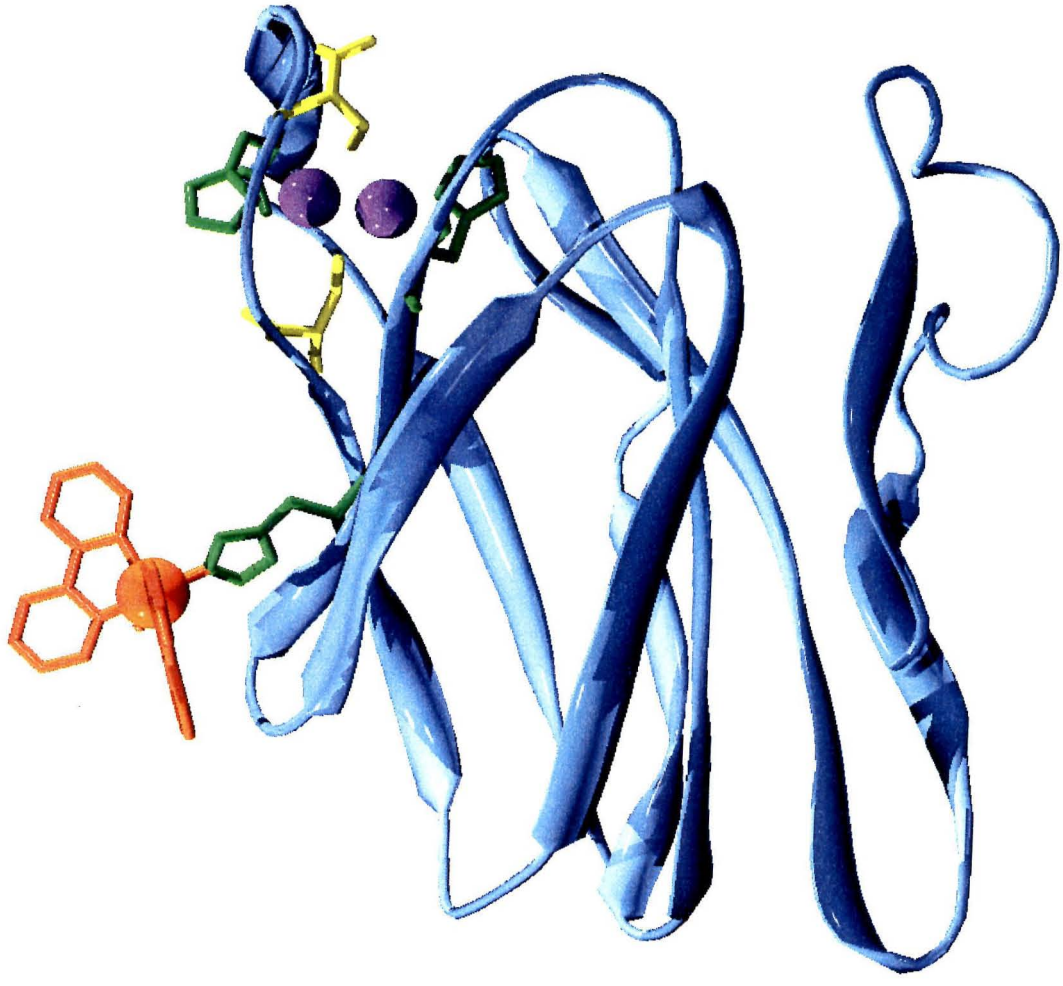

Figure 2.4. Electronic absorbance spectrum of the soluble Cu_A domain

The inset spectrum corresponds to the right-hand scale.

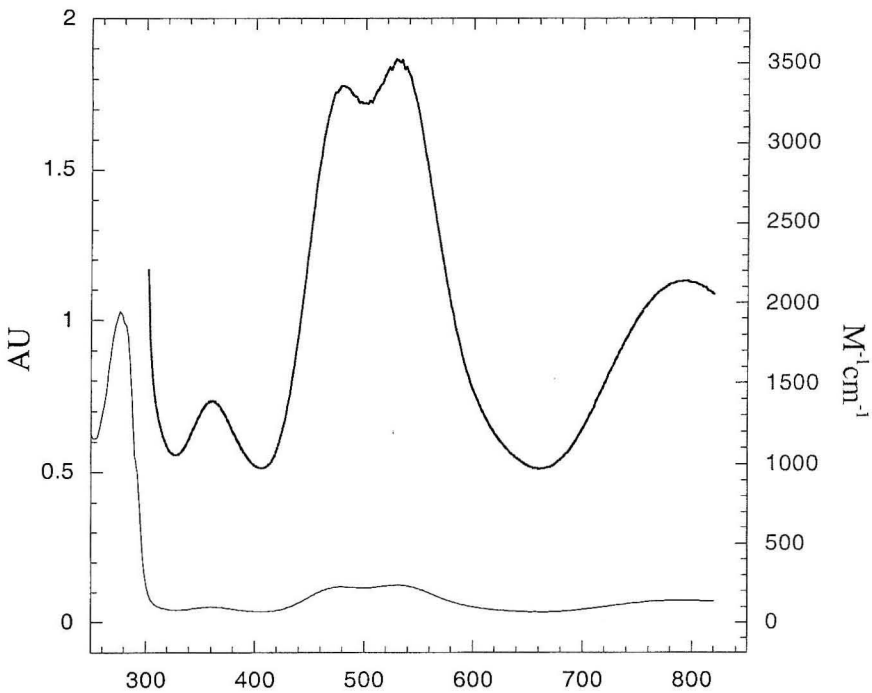
AU
$M^{-1}cm^{-1}$
2
1.5
1
0.5
0
3500
3000
2500
2000
1500
1000
500
0
300
400
500
600
700
800

Figure 2.5. Ruthenium modification of Cu_A

$Cu_A + Ru(bpy)_2CO_3 \longrightarrow Ru(bpy)_2(H_2O)(HisCu_A)$

imidazole

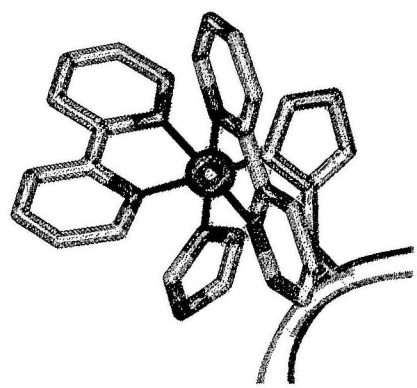

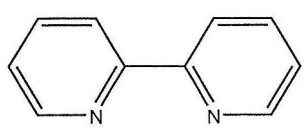

bpy

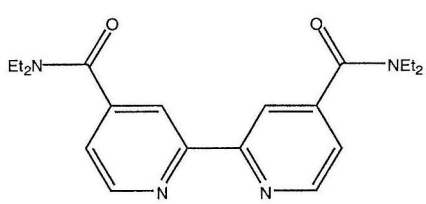

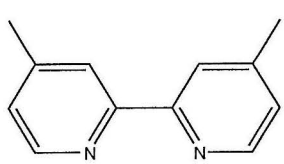

Me_2bpy

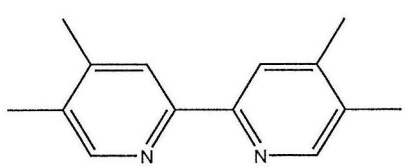

Me_4bpy

Figure 2.6. Model spectrum of $Ru(bpy)_2(im)Cu_A$

The solid line is the molar absorption spectrum of the unlabeled protein, the dotted line is that of the $Ru(bpy)_2(im)_2^{2+}$ model compound, and the dashed line is the sum of the two.

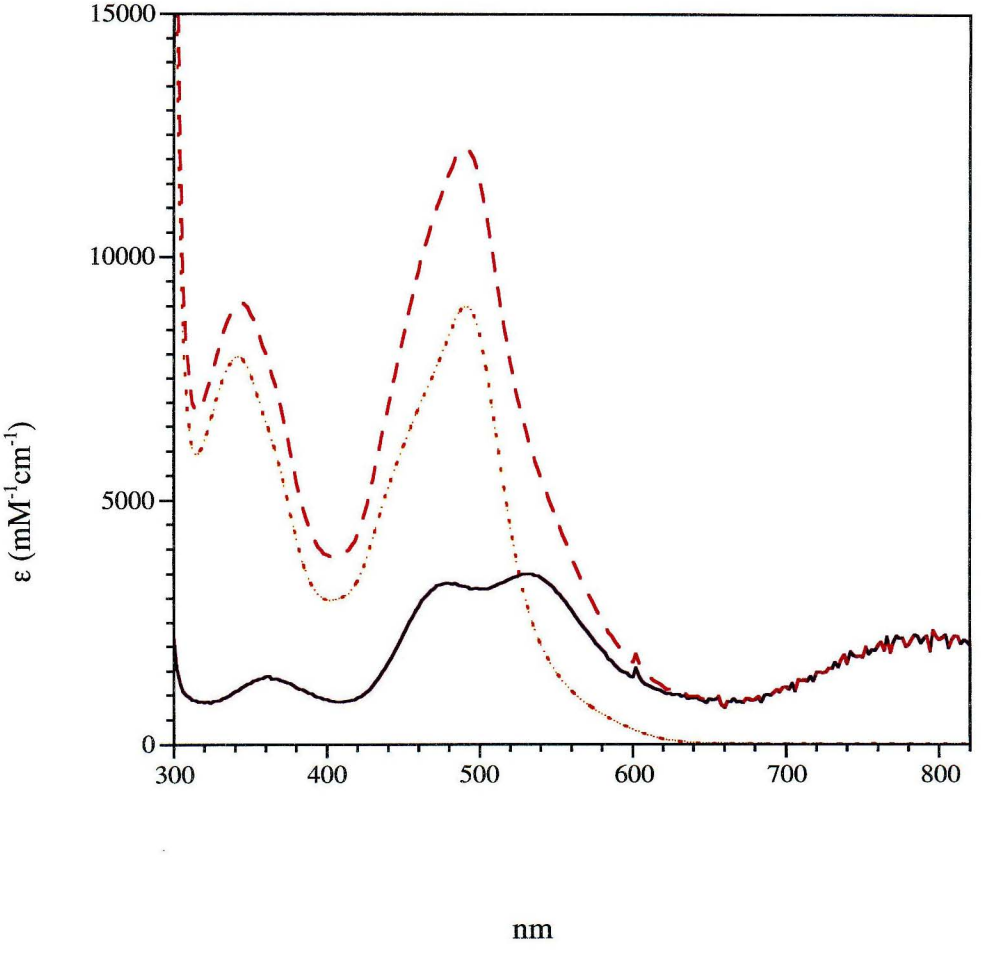
15000
10000
5000
0
300
400
500
600
700
800
ε (mM-1cm-1)
nm

Figure 2.7. Calculated difference spectrum for $Ru(III)Cu_A(red) - Ru(II)Cu_A(ox)$ (solid line) This is obtained by subtracting the oxidized Cu_A spectrum from the $Ru(bpy)_2(im)_2^{3+}$ – $Ru(bpy)_2(im)_2^{2+}$ difference spectrum (dashed line). It is not necessary to incorporate reduced Cu_A as it has an absorbance of zero over the range shown.

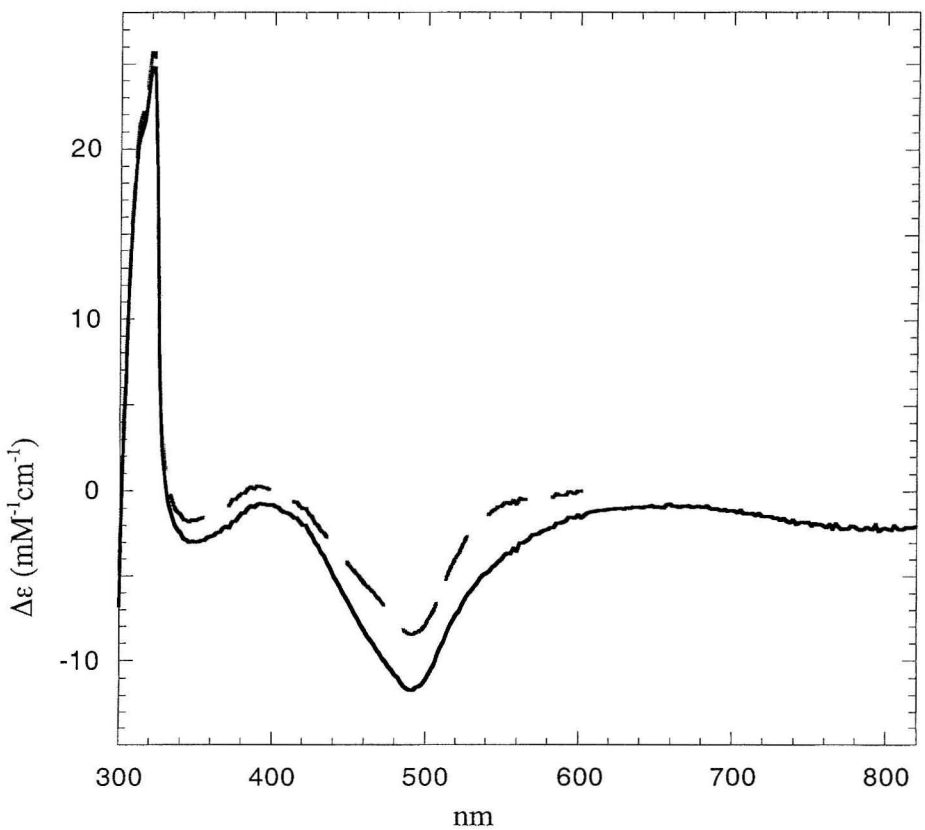
20
10
0
-10
Δε (mM-1cm-1)
300
400
500
600
700
800
nm

Figure 2.8. Photoinduced intramolecular flash-quench reaction

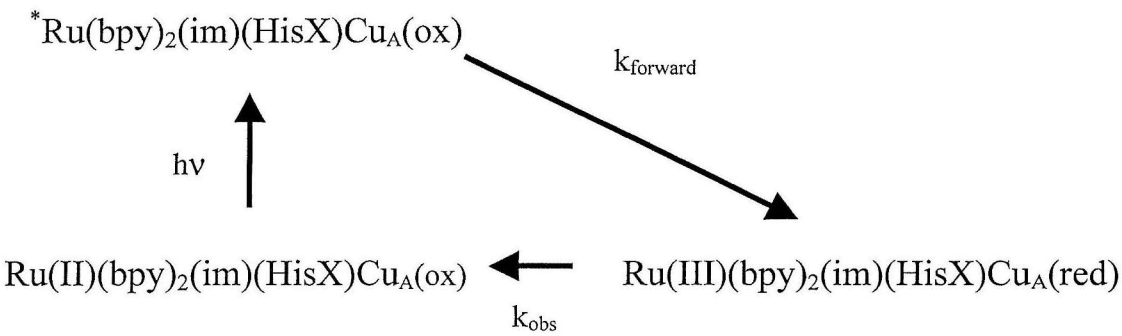
*Ru(bpy)2(im)(HisX)CuA(ox)
kforward
hν
Ru(II)(bpy)2(im)(HisX)CuA(ox)
Ru(III)(bpy)2(im)(HisX)CuA(red)
kobs

Figure 2.9. Transient absorption spectroscopy for $Ru(bpy)_2(im)His119Cu_A$

Observations at 431 nm, 530 nm, and 810 nm give an average rate of 2.28(2) $x10^5$ s^{-1}.

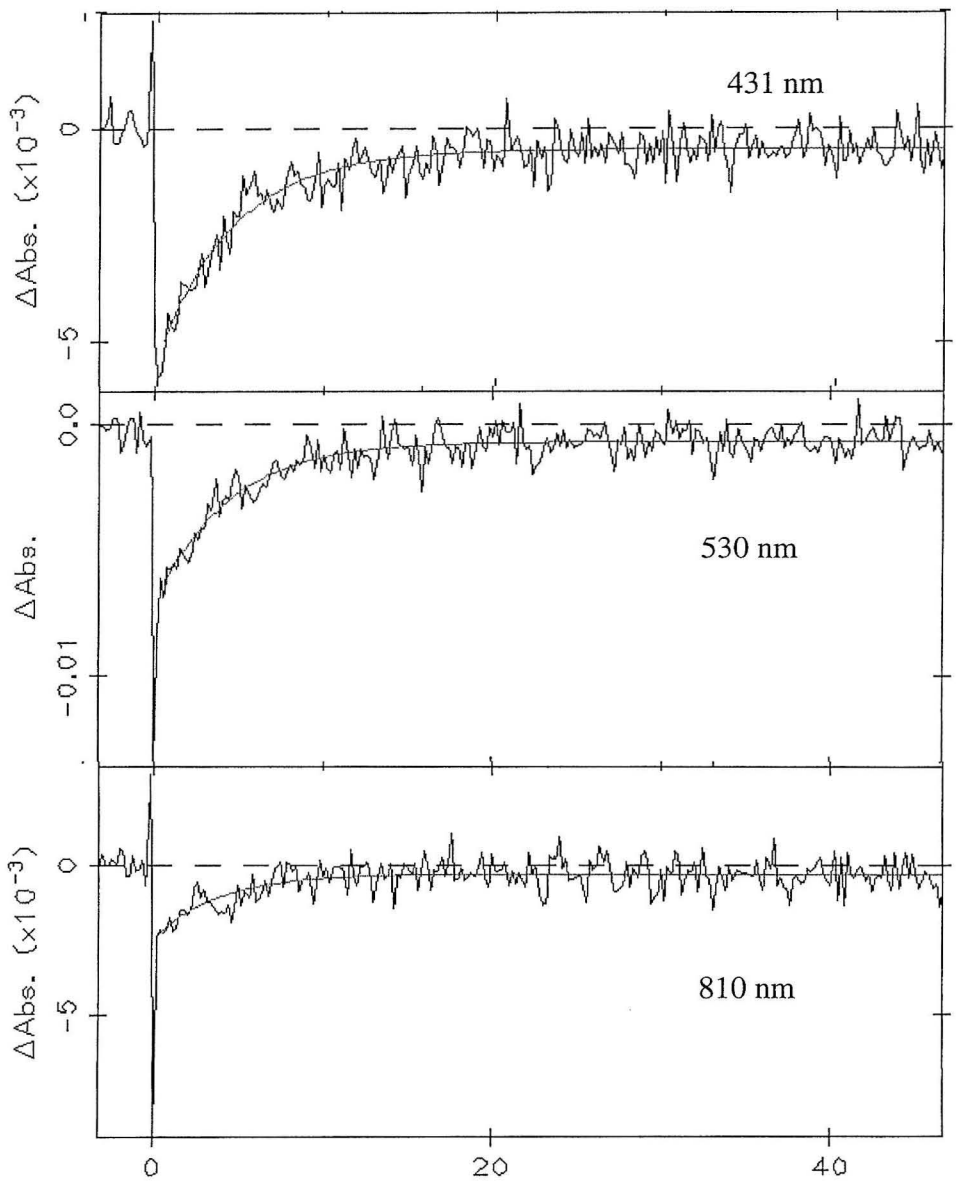
431 nm
530 nm
810 nm
ΔAbs. (x10⁻³)
ΔAbs.
0
-5
0.0
-0.01
20
40
μs

Figure 2.10. Transient absorption spectroscopy for $Ru(Me_4bpy)_2(im)His119Cu_A$

Observations at 431 nm, 530 nm, and 810 nm give an average rate of 3.3(3) $x10^5$ s^{-1}.

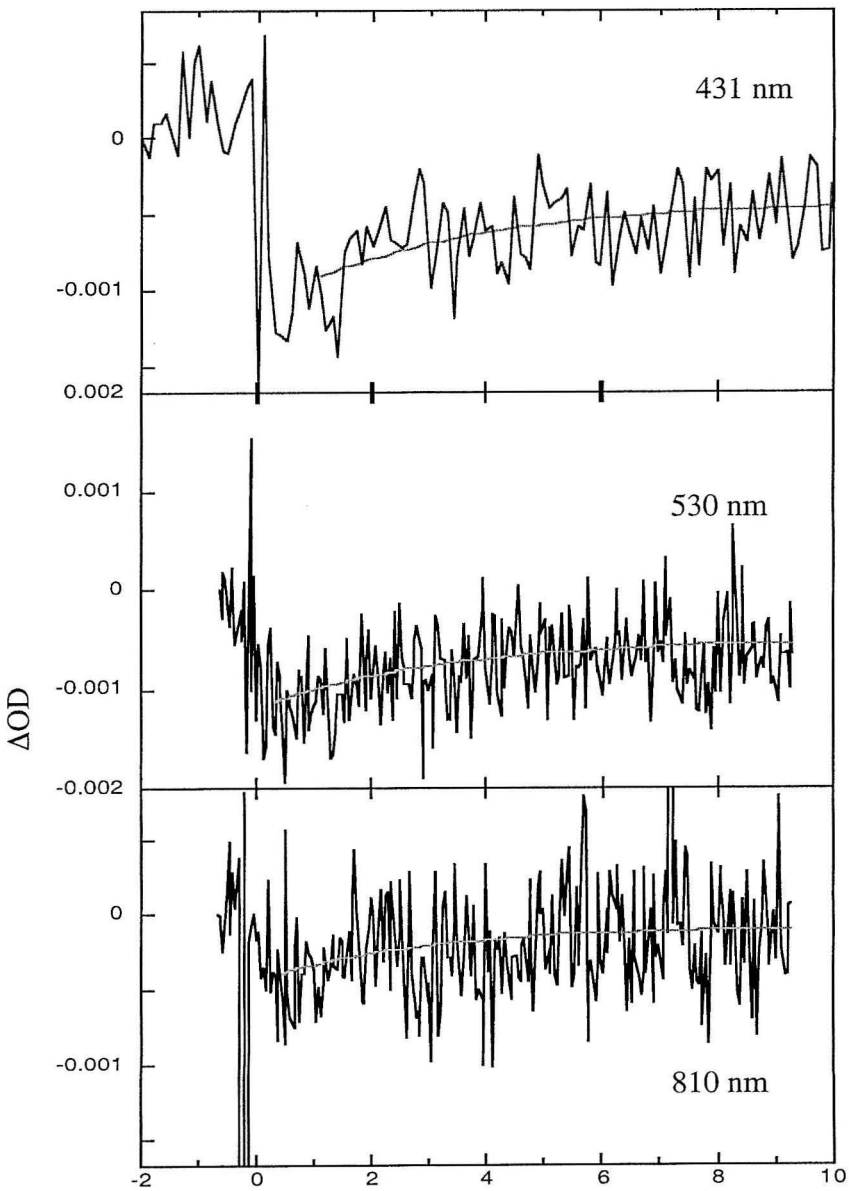
431 nm
530 nm
810 nm
0
-0.001
0.002
0.001
-0.002
ΔOD
-2
0
2
4
6
8
10
μs

Figure 2.11. Transient absorption spectroscopy for $Ru(Me_4bpy)_2(H_2O)His119Cu_A$

Observations at 318 nm, 430 nm, and 800 nm give a rate of $64 \pm 1\ s^{-1}$.

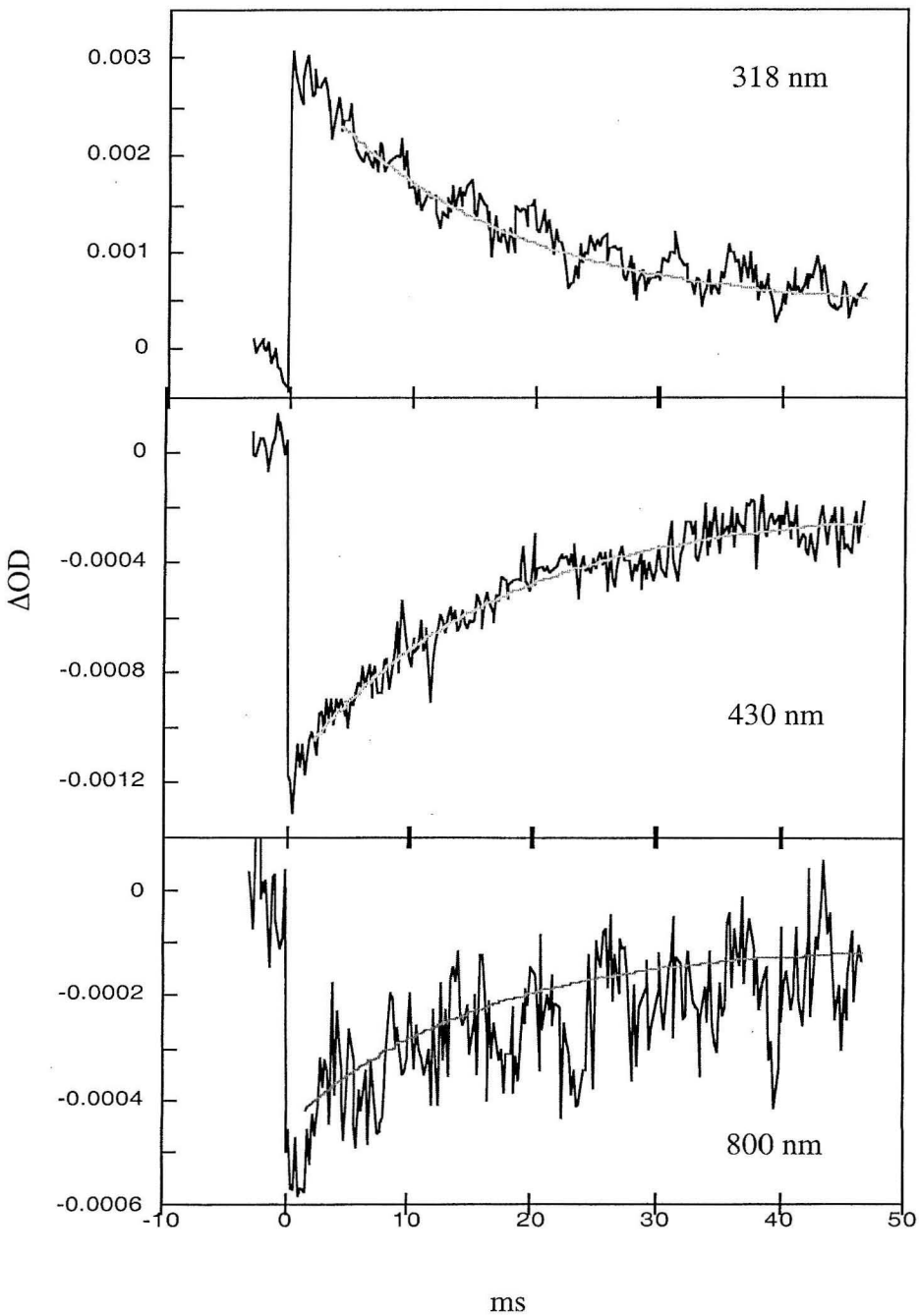
318 nm
430 nm
800 nm
ΔOD
ms
0.003
0.002
0.001
0
-0.0004
-0.0008
-0.0012
-0.0002
-0.0006
-10
10
20
30
40
50

Figure 2.12. Dependence of ET rates on driving force in His119Cu_A using the semiclassical ET equation (shown beneath the plot)

Driving forces take into consideration the shift in ruthenium reduction potential upon protein binding. The three inverted parabolas, from left to right, correspond to λ_{CuA} values of 0.4 eV, 0.6 eV and 0.8 eV. The best fit to the data was obtained for the middle curve (λ_{total} = 0.73 eV, H_{AB} = 0.03 cm^{-1}).

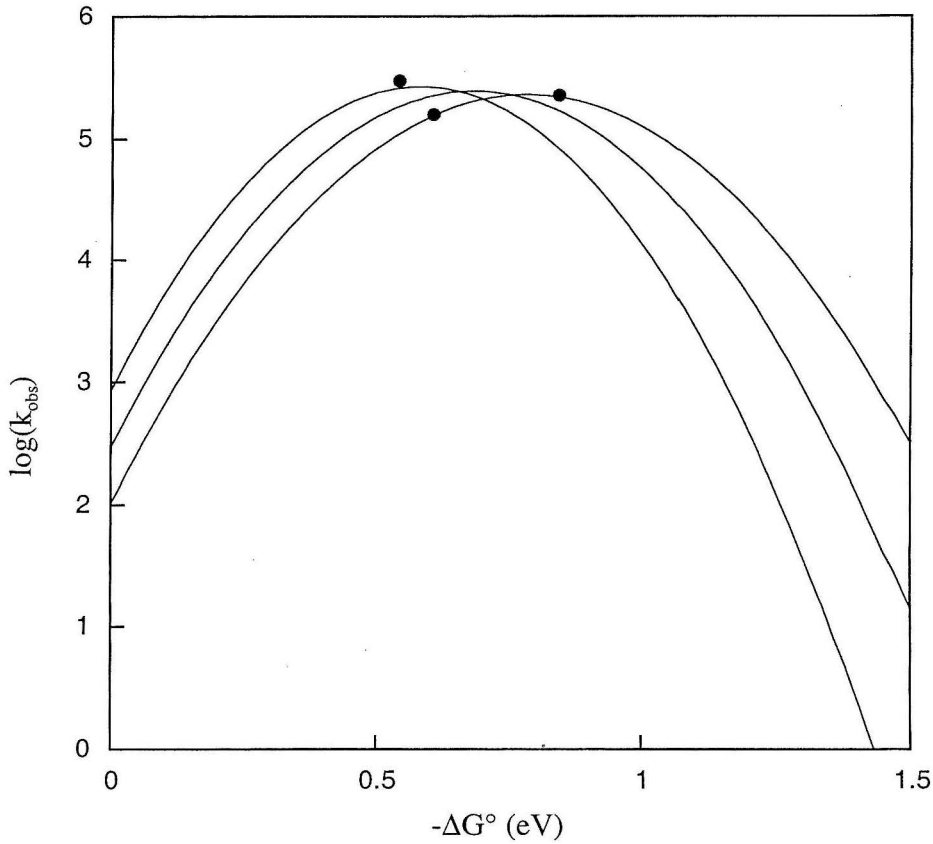

$$k_{ET} = \left(\frac{4\pi^3}{h^2 \lambda k_B T}\right)^{1/2} (H_{AB})^2 e^{\frac{-(\Delta G^\circ + \lambda)^2}{4\lambda k_B T}}$$

Figure 2.13. Comparison of solvent accessibility for two Cu_A centers

Dotted regions show the solvent accessible surfaces for histidines in purple Cu_A azurin (upper left) and in the soluble Cu_A domain from *T. thermophilus* (lower right).

Chapter 3

Role of Electron Tunneling Pathways in Cu_A

Introduction

The simplest interpretations of intramolecular electron transfer (ET) in proteins involve one of two models. In one, electron tunneling is viewed as passing directly through the protein matrix with the electronic coupling dependent on the donor-acceptor separation. This view predicts rates that decrease exponentially with distance, with a decay constant of about 1.4 $Å^{-1}$.[1] However, observed intramolecular ET rates do not always correlate strictly with a direct distance relationship.[2] Such instances support a model that emphasizes through-bond connectivities to form "tubes" or "pathways" for ET.[3,4]

In this model, electron transfer occurs primarily through covalently linked atoms, although hydrogen bonds and "jumps" between non-bonded atoms can be exploited as required. All of the individual elements are then taken together to give an overall coupling term. This can also be viewed in terms of an effective coupling distance, based on the number and types of bonds. While there is much experimental work supporting this refined model of ET,[5-7] there is still some question as to whether the available data has sufficient experimental certainty to prove either model conclusively.[8]

In this work, measurements of intramolecular ET in ruthenium-modified Cu_A from *T. thermophilus* give rates that do not vary as expected with the estimated donor-acceptor distances. This result can be interpreted in terms of the pathways model, with special attention paid to the nature of the hydrogen bonds linking adjacent beta-strands.

Materials and Methods

The expression and purification of His117 and His119Cu_A were performed as in Appendix A and ruthenium adducts were prepared as in Chapter 2. ET rates were measured by laser flash spectroscopy, also discussed in Chapter 2. HARLEM pathways analysis software was obtained from Dr. Igor Kurnikov, University of Pittsburgh.

Results and Discussion

ET rates in His117 and His119Cu_A

The ET rates in His117Cu_A were measured in the same manner as for His119 (Chapter 2). However, the intramolecular ET rate for Ru(bpy)$_2$(im)His117Cu_A is faster than for RuHis119Cu_A and is comparable with the excited state decay rate. As a result, it was necessary to measure luminescence decay rates for both the imidazole bound (4.2 x 10^7 s^{-1}) and aquo form (8.7 x 10^6 s^{-1}) of the ruthenium label and use those results in analysis of the transient absorption data (Figures 3.1 and 3.2). At 5.3(3) x 10^6 s^{-1}, the ET rate is ≈ 20 times faster for Ru(bpy)$_2$(im)H117Cu_A than for Ru(bpy)$_2$(im)H119Cu_A.

From studies of ET in azurin,[6,9] it is seen that a displacement by two amino acid positions can change the ET rate by a factor of ≈ 300. If this were always the case, the rate in RuH119Cu_A would be too fast – or else the rate in RuH117Cu_A too slow – by a factor of 15. Taking the relative donor-acceptor distances, 14.3 Å for 117 and 18.3 Å for 119, from RuCu_A models created in Insight II predicts a ratio of about 270 when using a strict distance decay of 1.4 $Å^{-1}$.[1] However, the work with azurin also found exceptions where an observed rate at a certain position on the protein was substantially faster than expected. This was explained in terms of the pathways model for intramolecular ET in proteins.[3,5,10]

Hydrogen bonds and pathways in RuCu_A

In the pathways model, discrete through-bond paths connecting donor to acceptor are used to explain ET rates. The overall electronic coupling for a path is then found from the product sum of the individual coupling terms for discrete coupling elements comprising the

path. Thus, each element in the series gives an adjustment to the overall coupling (H_{AB}) as follows:[3]

$$H_{AB} \propto \prod_i \varepsilon_C(i) \prod_j \varepsilon_H(j) \prod_k \varepsilon_C(k) \qquad \text{(Equation 1)}$$

$$\varepsilon_C = 0.6 \qquad \text{(covalent bonds)}$$

$$\varepsilon_H = (0.6)^2 e^{-1.7(R_H - 2.8)} \qquad \text{(hydrogen bonds)}$$

$$\varepsilon_S = \frac{1}{2}(0.6) e^{-1.7(R_S - 1.4)} \qquad \text{(through-space jumps)}$$

Covalent bonds provide the strongest coupling, but hydrogen bonds are considered approximately the same as two covalent bonds (i.e., N—H—O), adjusted for any deviation from the average N—O distance of 2.8 Å. Through-space jumps are the weakest coupling element, with a severe distance dependence. Note that this simple model treats metal-ligand bonds as equivalent to carbon-carbon bonds and an adjustment is needed to compensate for differences in covalency for different metal-ligand bonds.

The beta-strands in azurin form such pathways and the hydrogen bonds connecting them provide a means to cross from one strand to another. As a result, the different degrees of electronic coupling to the metal for the different ligands in the active site can be exploited. For example, a pathway involving a strand leading to a cysteine ligand may be better coupled to the copper center than one on a strand leading to a histidine or methionine.

A similar interpretation can be used to explain the observed ratio of rates in $RuCu_A$. Positions 117 and 119 are on a strand that leads to His114. If the pathway from His119 instead crosses over via a hydrogen bond to the strand bearing Cys149, the decrease in coupling due to use of the hydrogen bond will be offset by the increase in coupling due to 6 fewer covalent bonds in the path and the use of cysteine relative to histidine (Figure 3.3). Still, it can be seen that an ET path to position 117 could also exploit a hydrogen bond to

connect with Cys149. Simply adjusting for the differences in bond length among the hydrogen bonds connecting the two strands is not sufficient to explain the low ratio of rates for the two positions.

However, other geometric parameters for that single hydrogen bond to position 117 are far from optimum, whereas the additional hydrogen bonds available for coupling to position 119 are closer to the ideal (Figure 3.3). Not only does the hydrogen bond leading to position 117 have a longer N—O distance (3.0 Å) than average, but also the orientation of the carbonyl and the amide are offset in such a way as to diminish the overlap of the appropriate orbitals. It seems reasonable that geometric parameters other than length may influence the electronic properties the hydrogen bond.

Angular factors on hydrogen bond properties

As the position of the hydrogen atom is generally not observed, a set of coordinates based on the heavy atom positions is needed to define the hydrogen bond. As shown in Figure 3.4, the colinearity and coplanarity of the N—H and C=O bonds can be described in terms of the angles α, $\delta 1$, and $\delta 3$, as defined by Cheam and Krimm.[11] In that computational work, variations in these angular parameters have the same effects on electronic properties of the hydrogen bond, such as dissociation energy and force constant, as do changes in the bond length, R.

The pathways model does not contain an adjustment for the effects of angular changes on a hydrogen bond. Indeed, in cases where the pathways model does not give an adequate description of experimental results, it is best to employ full *ab initio* methods to model all the orbitals in likely ET paths. However, using the tabulated calculations from literature,[11] one can find a primitive correlation between the deviation from the optimum

value for an angle and an increase in bond length. For example, an increase in $\delta 1$ from 0° to 5° results in the same change in calculated electronic properties as does an increase in bond length from 2.8 Å to 2.9 Å. According to the hydrogen bond term in the pathways model, this change in bond length should reduce the overall coupling by 15%, if all other factors are the same. Therefore, it seems likely that the corresponding change in bond angles would have a similar influence, at least for small deviations from the average values.

Applying this approach to the $RuCu_A$ system greatly reduces the coupling element of the hydrogen bond for the His117 pathway. Neither hydrogen bond is perfectly aligned (i.e., $\delta 1 \approx 60°$, $\delta 2 = 0°$), but the other parameters for the best hydrogen bond leading to position 119 are not far from optimum. On the other hand, the hydrogen bond to position 117 is long (3.0 Å) and lacks coplanarity ($\delta 3 = 18°$). This degree of coplanarity leads to predicted electronic properties that are comparable to those of a 3.4 Å hydrogen bond, all other factors being ideal. From the exponential decay term in the coupling element for a hydrogen bond (i.e., $e^{-1.7(R-2.8)}$), this would suggest an additional 64% reduction in coupling.

The lack of alignment and planarity in this one hydrogen bond makes the coupling for the pathway connecting position 117 to Cys149 only 20% greater than that to His114, not considering the greater Cu-S coupling. With the increased Cu-S coupling, the total coupling is over 20 times greater using Cys149 rather than His114. This indicates that the best pathway to position 117 probably does cross over from the cysteine strand. However, the coupling to position 119 can utilize additional hydrogen bonds, including one of nearly optimum geometry. As a result, the coupling of the active site to position His117 is predicted to be at most 5.5 times greater than to position 119. This corresponds to a ratio of rates of 30, comparable to the observed ratio of 20.

Pathways in cytochrome oxidase

The crystal structure for cytochrome oxidase from *T. thermophilus*[12] reveals a pathway from the Cu_A site to heme *b* (analogous to heme *a* in mammalian systems) that utilizes His157 (Figure 3.5), in the same manner as the first pathway proposed for the bovine oxidase.[13,14] Other pathways have been proposed for the bovine system utilizing the cysteine residues.[15,16] Such pathways would offset the increase in the bond count and/or the utilization of through-space jumps with the increased coupling to cysteine relative to histidine in the active site. There is no indication of a viable alternate pathway in the *T. thermophilus* structure. The second best pathway, through Cys153, predicts a 100-fold slower rate, even after incorporating a 20-fold greater coupling of cysteine relative to histidine. It seems more likely that cysteine is to be implicated in the injection of electrons into the Cu_A site from cytochrome *c*, not in the subsequent transfer to heme *b*.

Conclusion

The simple pathways model does not explain the ratio of rates for intramolecular ET from the copper site to residues 117 and 119 in the soluble Cu_A domain from *T. thermophilus*. It would appear that in cases such as this, a more comprehensive approach is required, taking into account all of the geometric factors, including angles, defining the distribution of atoms and bonds in the system. A very simple approach indicates that the coupling for a path from Cys149 to position 117 involving a distorted hydrogen bond would be comparable to the path from His114, keeping to the same strand. The diminished coupling due to this hydrogen bond can explain the apparent slowness of ET in RuHis117Cu_A relative to RuHis119Cu_A. Without incorporating the relative Cys/His coupling, it is not possible to assess conclusively if ET to position 117 involves a hydrogen

bond crossing to cysteine. However, as no corrections other than the relative couplings of the available hydrogen bonds are necessary, it would appear that the two paths do involve the same metal-ligand interaction and therefore coupling to cysteine appears more likely. However, enhanced coupling of copper to cysteine relative to histidine does not appear to be sufficient to overcome all situations: ET from Cu_A to heme *b* in the *T. thermophilus* oxidase probably involves His157.

References

(1) Moser, C. C.; Page, C. C.; Chen, X.; Dutton, P. L. *J. Biol. Inorg. Chem.* **1997**, *2*, 393-398..

(2) Winkler, J. R.; Gray, H. B. *J. Biol. Inorg. Chem.* **1997**, *2*, 399-404.

(3) Beratan, D. N.; Onuchic, J. In *Protein Electron Transfer*; Bendall, D. S., Ed.; BIOS Scientific Publishers Ltd.: Oxford, 1996; pp 23-42.

(4) Regan, J. J.; Onuchic, J. N. In *Electron Transfer-from Isolated Molecules to Biomolecules, Pt 2*, 1999; Vol. 107, pp 497-553.

(5) Beratan, D. N.; Onuchic, J. N.; Betts, J. N.; Bowler, B. E.; Gray, H. B. *J. Am. Chem. Soc.* **1990**, *112*, 7915-7921.

(6) Regan, J. J.; Dibilio, A. J.; Langen, R.; Skov, L. K.; Winkler, J. R.; Gray, H. B.; Onuchic, J. N. *Chem. Biol.* **1995**, *2*, 489-496.

(7) Farver, O.; Pecht, I. *J. Biol. Inorg. Chem.* **1997**, *2*, 387-392.

(8) Williams, R. J. P. *J. Biol. Inorg. Chem.* **1997**, *2*, 373-377.

(9) Langen, R. Thesis: "Electron Transfer in Proteins: Theory and Experiment," California Institute of Technology, 1995.

(10) Onuchic, J. N.; Beratan, D. N.; Winkler, J. R.; Gray, H. B. *Annu. Rev. Biophys. Biomolec. Struct.* **1992**, *21*, 349-377.

(11) Cheam, T. C.; Krimm, S. *J. Mol. Struct.* **1986**, *146*, 175-189.

(12) Soulimane, T.; Buse, G.; Bourenkov, G. P.; Bartunik, H. D.; Huber, R.; Than, M. E. *Embo J.* **2000**, *19*, 1766-1776.

(13) Ramirez, B. E.; Malmström, B. G.; Winkler, J. R.; Gray, H. B. *Proc. Natl. Acad. Sci. U. S. A.* **1995**, *92*, 11949-11951.

(14) Regan, J. J.; Ramirez, B. E.; Winkler, J. R.; Gray, H. B.; Malmstrom, B. G. *J. Bioenerg. Biomembr.* **1998**, *30*, 35-39.

(15) Gamelin, D. R.; Randall, D. W.; Hay, M. T.; Houser, R. P.; Mulder, T. C.; Canters, G. W.; de Vries, S.; Tolman, W. B.; Lu, Y.; Solomon, E. I. *J. Am. Chem. Soc.* **1998**, *120*, 5246-5263.

(16) Medvedev, D. M.; Daizadeh, I.; Stuchebrukhov, A. A. *J. Am. Chem. Soc.* **2000**, *123*, 5757-5767.

Table 3.1. Intramolecular ET rates at 25 °C for $Ru(bpy)_2(im)His117Cu_A$ and $Ru(bpy)_2(im)His119Cu_A$

Complex	Luminescence decay constant (s^{-1}), aquo	Luminescence decay constant (s^{-1}), im	k_{ET} (s^{-1})
$Ru(bpy)_2(im)H119Cu_A$	N/A	1.6×10^7	$2.28(2) \times 10^5$
$Ru(bpy)_2(im)H117Cu_A$	4.7×10^7	8.4×10^6	$5.9(4) \times 10^6$

Figure 3.1. Emission decay for $Ru(bpy)_2(H_2O)His117Cu_A$ (top) and $Ru(bpy)_2(im)His117Cu_A$ (bottom)

The decay for the imidazole complex is biphasic, with one component corresponding to the decay for the aquo complex ($4.7 \times 10^7\ s^{-1}$) and the other to the decay for the imidazole complex ($8.4 \times 10^6\ s^{-1}$). Fits are determined by deconvolution from the instrument response, and are shown here with the raw data.

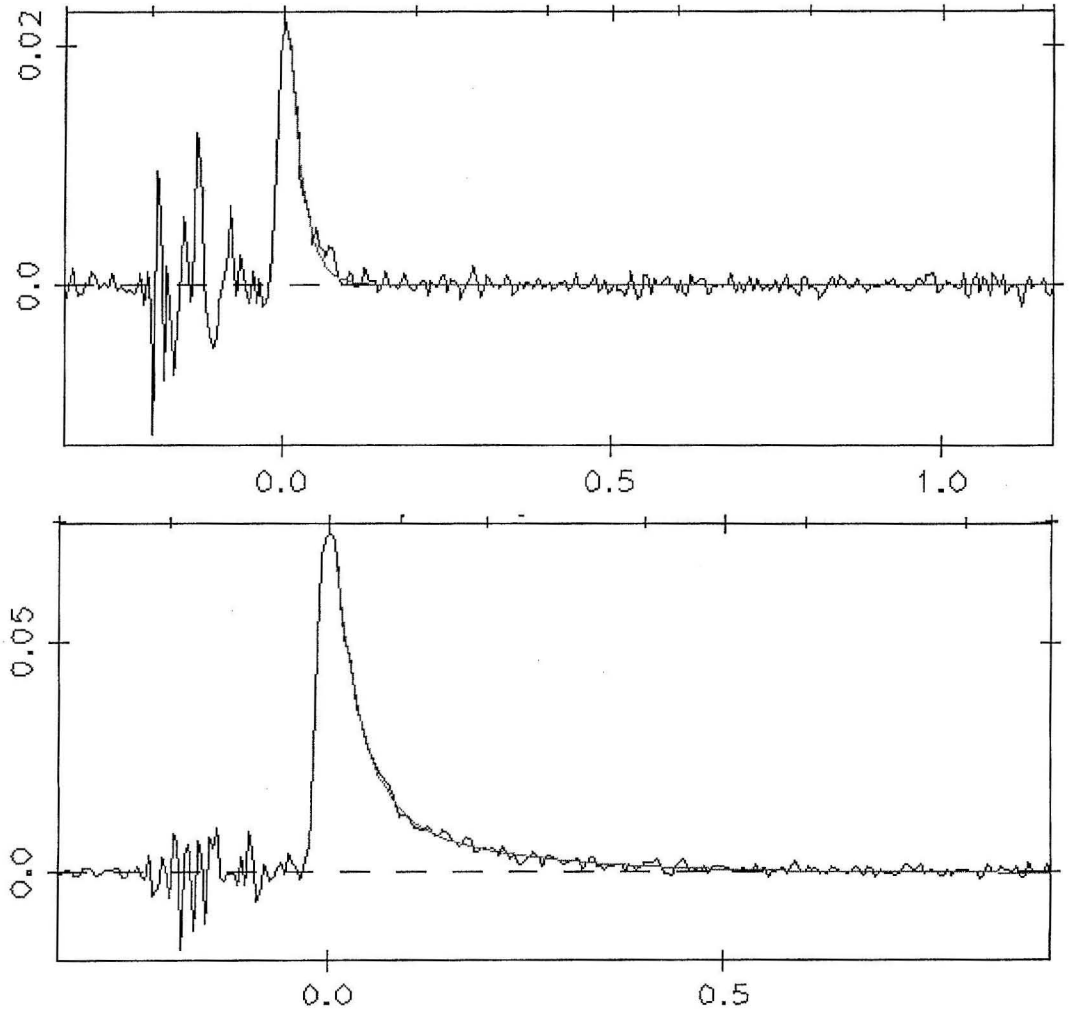

Intensity

μs

Figure 3.2. Single wavelength kinetics for $Ru(bpy)_2(im)His117Cu_A$

Curve fits incorporate fixed values for the excited state decay, as determined from the emission lifetime. Rates measured at 430 nm, 530nm, and 800 nm give an average of $5.9(4) \times 10^6\ s^{-1}$.

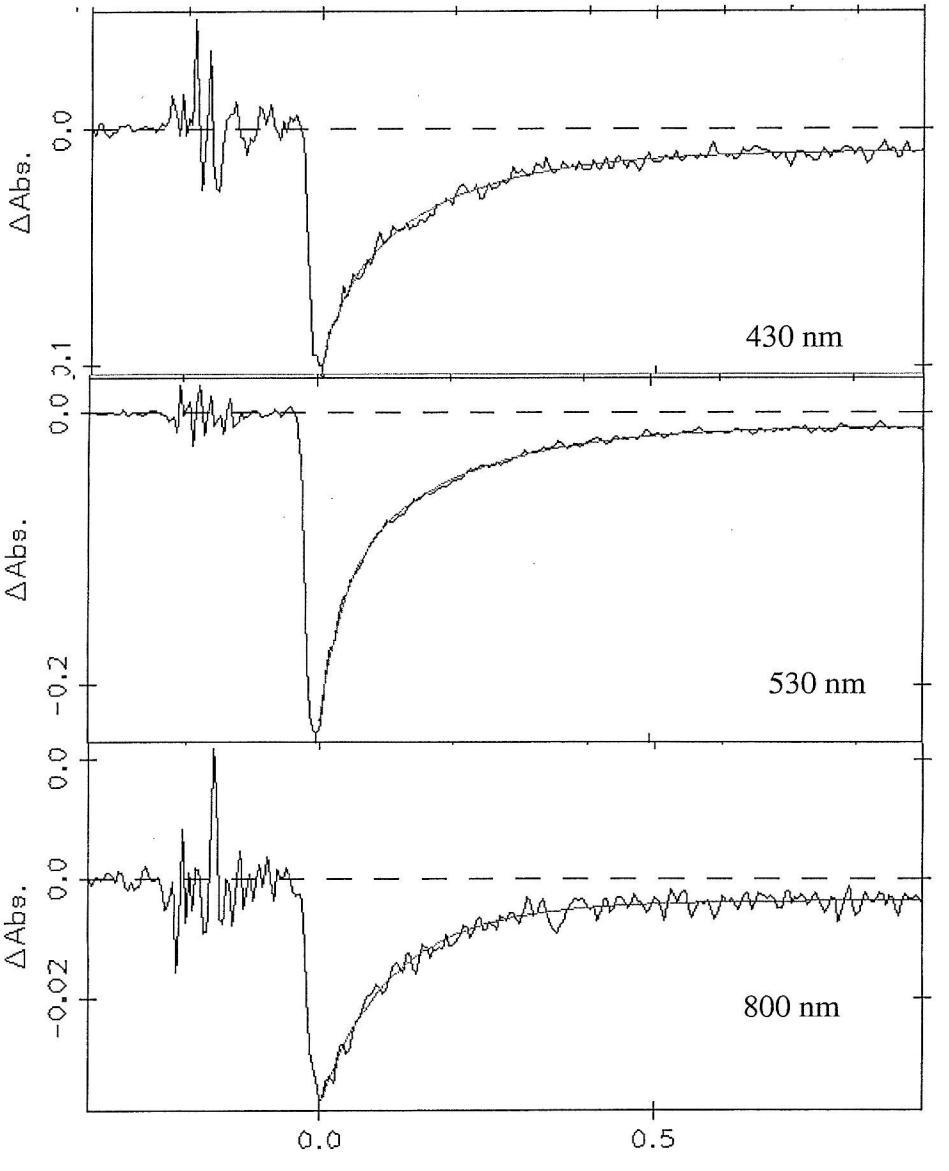
ΔAbs.
0.0
0.1
430 nm
ΔAbs.
0.0
-0.2
530 nm
ΔAbs.
0.0
0.0
-0.02
800 nm
0.0
0.5
μs

Figure 3.3. Pathways in $RuCu_A$

Shown here are two perspectives of the pathways leading from the dicopper site to positions 117 and 119 (for the sake of illustration both residues are depicted as histidine, with a ruthenium label at position 119). Note the hydrogen bonds between the strands leading to His114 and Cys149. The leftmost is the only one available to link position 117 with Cys149 and is poorly aligned (denoted by arrow in lower illustration).

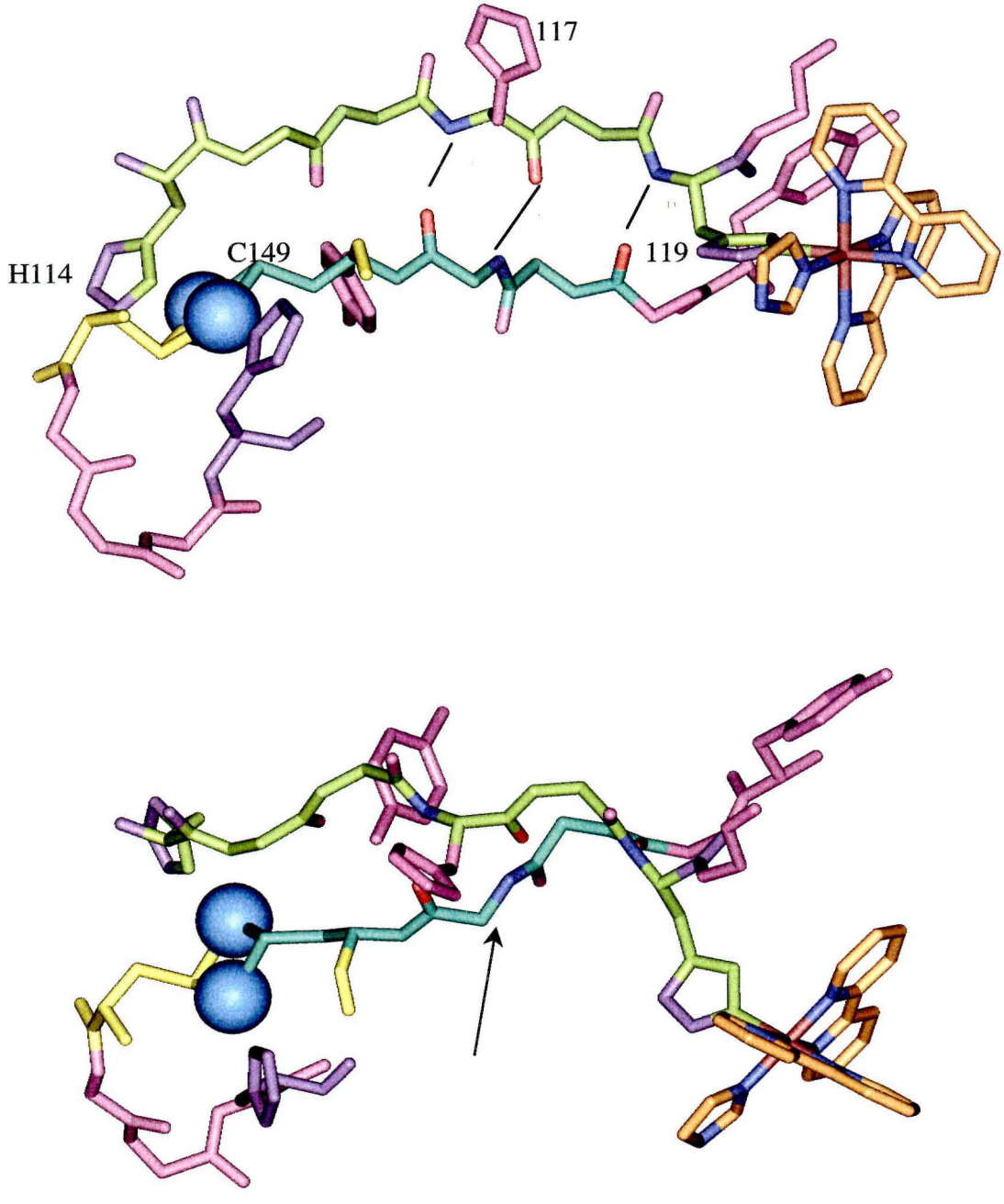
117
H114
C149
119

Figure 3.4. Hydrogen bonds and ET pathways in $RuCu_A$

The pathway in $RuHis119Cu_A$ can utilize a hydrogen bond (A and C) that is much closer to the ideal orientation than the one (B and D) available to the pathway in $RuHis117Cu_A$.

A)

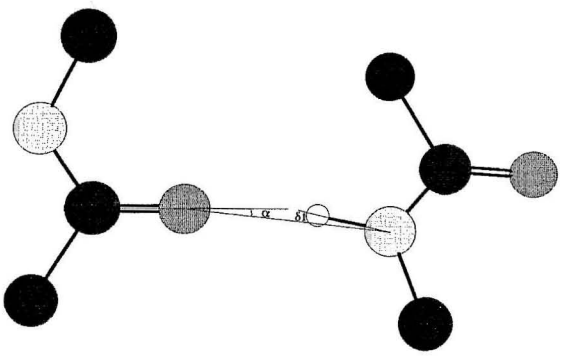

B)

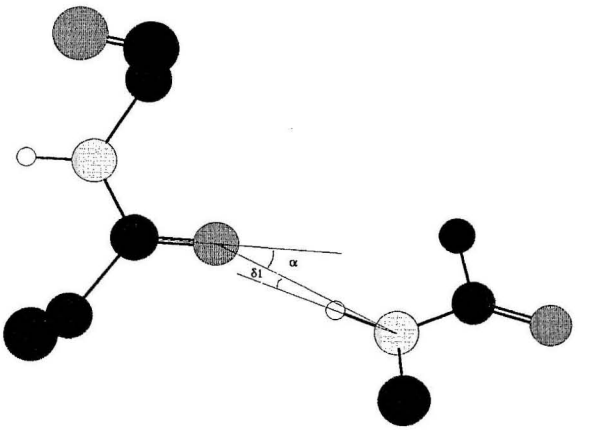

C)

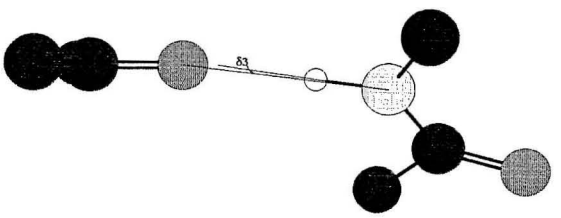

D)

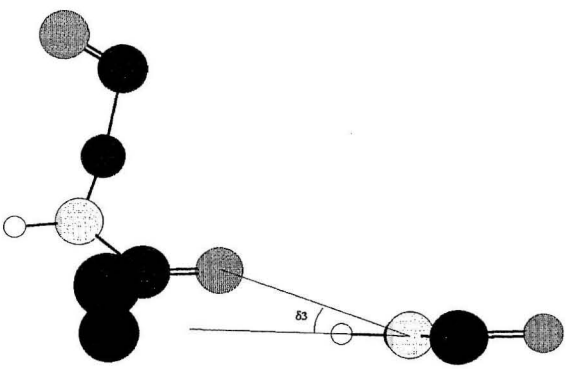

Figure 3.5. Pathways from the Cu_A site to heme *b* in cytochrome *c* oxidase from *T. thermophilus*

Dotted lines indicate hydrogen bonds, dashed lines through-space jumps. The predicted best path is down the center, through His157. The next best alternative is on the right-hand side of the figure, leading from Cys153 to Tyr152, then a jump to Arg450 of Subunit II.

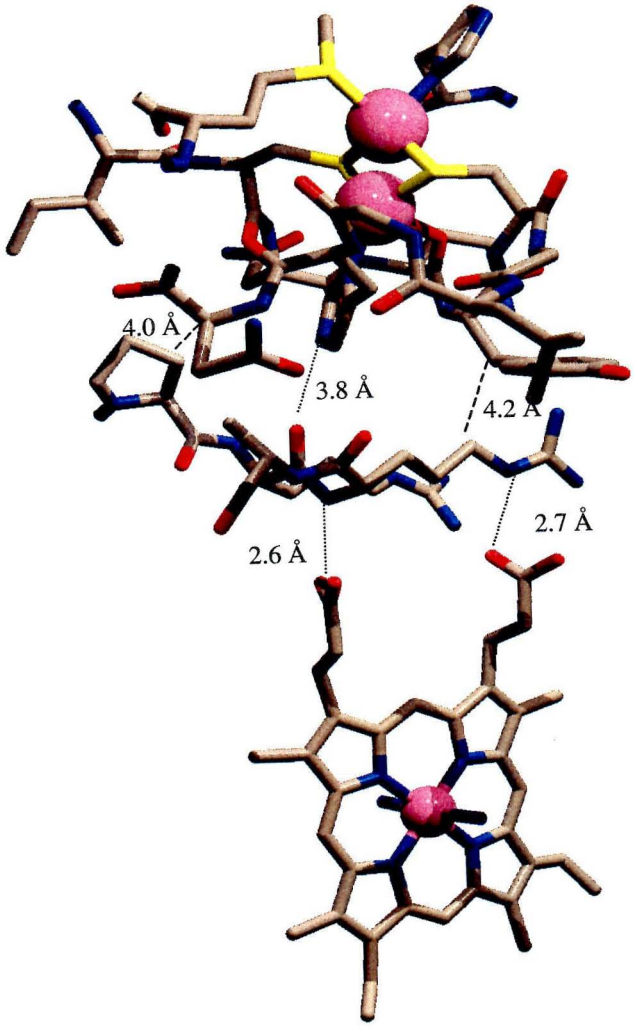
4.0 Å
3.8 Å
4.2 Å
2.7 Å
2.6 Å

Chapter 4

H/D Isotope Effects on ET in Azurin

Introduction

The application of the pathways model[1-3] to intramolecular ET in copper proteins indicates that hydrogen bonds may have important roles in the electronic coupling between donor and acceptor.[4,5] Ratios of ET rates involving different locations in ruthenium-modified azurin suggest that crossings occur between adjacent strands, presumably via hydrogen bonds. Within this model, intramolecular ET in RuHis83azurin (Figure 4.4) certainly requires the mediation of hydrogen bonds, as any all-covalent bond path is too circuitous.

Deuterium incorporation is one means to change the electronic properties of a hydrogen bond. An increase in strength and very slight decrease in length are expected for relatively weak hydrogen bonds such as those typically found in peptide backbones.[6,7] Some caution is required in the interpretation of any results. Short, strong hydrogen bonds are occasionally found in peptides[8] and exhibit the opposite changes in length and strength upon deuteration.[9-11]

In order to investigate the role of hydrogen bonds in intramolecular ET in azurin, a deuterium incorporation strategy was devised. In principle, stronger hydrogen bonds within a pathway may give greater electronic coupling, as evidenced by stiffer vibrational modes upon deuteration.[7] However, an increase in the strength of the hydrogen bonds in the solvent cage surrounding the protein may lead to an increase in the solvent reorganization energy. Such opposing effects would make it difficult to interpret the outcome. However, the strategy presented here will exploit the varying H/D exchange rates in azurin[12] to control for solvent/outer-sphere isotope effects.

Materials and Methods

General

The basic methods for manipulating azurin are similar to those given in Appendix A for Cu_A. As was the case for Cu_A, azurin was expressed from cell stocks created in the laboratory of Prof. John H. Richards at Caltech.[13] Some purified azurin samples were prepared by and with Dr. Angelo Di Bilio.

Purification of wild-type azurin

Azurin from *P. aeruginosa* was expressed in *E. Coli* (BL21(DEA3)) grown on LB media supplemented with 30 mg/L kanamycin. This construct uses periplasmic expression, so recovery of the protein was done using osmotic shock rather than cell lysis. After harvesting by centrifugation, the cells were resuspended by shaking for 20 minutes at 5°C, using 1/5th the original culture volume of 30 mM Tris•HCl with 1 mM EDTA and 20% sucrose, pH = 8. The cells were then pelleted again by centrifugation at 5000 rpm for 10 minutes. The sucrose fraction was discarded, as it was found to contain minimal quantities of azurin from cell lysis. The pellet was then suspended in ice-cold water, or better, 5 mM $MgSO_4$, also at 1/5th the original culture volume. The cells were removed by centrifugation and $CuSO_4$ was added to the extrudate to a final concentration of 5 mM.

The azurin containing solution turned a deeper blue over time. The solution was concentrated using an Amicon and then subjected to chromatography. While it is possible to proceed directly to the FPLC, it was later found to be more effective to add acidic NaOAc buffer and run the protein down a 10 cm Fast-Flow CM-Sepharose column equilibrated in 20 mM NaOAc, pH = 4.5. The presence of $MgSO_4$ and excess copper would diminish binding,

but the dark blue azurin-containing fraction still exhibited an improved purity index as determined by electronic absorbance ($A_{630/280} \approx 0.6$). Either Mono S cation exchange (20 – 300 mM NaOAc, pH = 4.5) or Mono Q anion exchange (20 mM Tris•HCl, 0 – 200mM NaCl, pH = 8) FPLC chromatography was used for the final purification. Purification of the reduced form afforded a means to separate the Cu(I) form from any Zn(II) impurity.

N-15 enriched azurin was obtained in a similar manner, but using M9 minimal media[14] with double the amount of phosphate and supplemented with Eagle Basal Vitamin mix. 1 mL cultures were grown on LB first, then transferred to 50 mL volumes of minimal media, which were used to inoculate 1 L volumes. N-15 ammonium sulfate (Isotec) was used as the sole nitrogen source. The final yield was about 35 mg/L, though half of that was actually recovered from the medium rather than the osmotic extrudate. Following purification, the protein was characterized by UV-Vis ($R_{280/630} > 0.55$) and MALDI-TOF mass spectrometry ($M^+ = 14{,}110$ for apoprotein).

$Ru(bpy)_2$(im)(HisX)azurin, X = 83, 109

Ruthenium modification conditions were essentially the same as those given in Chapter 2. Samples were not considered air-sensitive and copper loss was not a problem, so incubations were done in sealed vials in the dark with greater concentrations of imidazole than were used for Cu_A (400 mM imidazole•HCl, pH = 7.5 with 100 mM NaCl and 10 mM CuSO4). IMAC chromatography was done as before; however, singly labeled azurin has little affinity for the column and requires purification by Mono S to separate it from the multiply labeled forms.

Wild-type azurin (His83) was found to react readily with $Ru(bpy)_2CO_3$, typically reaching completion within 24 hours. On the other hand, the His109 mutant takes much

longer, 7 – 10 days, possibly due to steric constraints at that position. These steric constraints may also be responsible for the shifted MLCT for the ruthenium label (from 490 nm to 486nm).

Deuteration reactions

Buffers using D_2O were kept in tightly closed containers, and glassware and electrodes used were first dried then rinsed with D_2O. pD values were obtained by adding 0.4 to the apparent pH.[15] Denaturant solutions were obtained by using a laboratory stock of solid guanidine hydrochloride, previously exchanged with D_2O and kept in tightly closed bottles. PD-10 gel filtration columns were rinsed with >30 mL D_2O and allowed to equilibrate for 24 hours before use, tightly sealed in the interim.

RuAzurin was exchanged into a deuterated buffer with three cycles of ultrafiltration (Centricon-10). Cumulative time until ET measurement was usually 6 – 12 hours. Some measurements were made after several weeks in the deuterated buffer. For more expedient exchange, the protein was titrated with dithionite, passed down a PD-10 gel filtration equilibrated with deuterated buffer to remove excess reductant, then unfolded with an equivalent volume of 8 M guanidinium chloride, pD = 7.5, in D_2O. After 15-20 minutes, the unfolded protein was passed down a gel filtration column to remove the denaturant. The deuterated protein was kept in deuterated buffer until ready for use. When it was necessary to exchange the buffer for one of a normal isotopic content, ultrafiltration was used as before.

Electrochemistry

Electrochemical measurements were obtained using an edge plane graphite electrode, polished successively with 0.3 μm and 0.05 μm alumina, sonicated in water for 15 minutes,

and dried with a heat gun. A three-arm cell was used, in which the sample chamber was separated from the platinum wire auxiliary electrode by a glass frit, and from the Ag/AgCl reference electrode by a modified Luggin capillary. For non-isothermal measurements, a 3 M KCl salt bridge was used to bridge the reference electrode at room temperature to the rest of the apparatus in a constant temperature bath.

Kinetic measurements

Rates of intramolecular electron transfer were measured as described in Chapter 2 Cu_A. However, in addition to monitoring signals at 430 nm and 530 nm corresponding to changes in ruthenium oxidation state, a HeNe laser was used to probe 632.8 nm, close to the LMCT for oxidized azurin. This afforded several advantages, including the ability to use irises to shield the detector from sources of scattered light and any reflected luminescence from the sample. In addition to measurements of direct intramolecular electron transfer with oxidized Ru-azurin, measurements were made with the reduced form of the protein using an exogenous quencher, $Ru(NH_3)_6Cl_2$, to generate $Ru(III)bpy_2(im)$azurin.

Results and Discussion

Deuteration procedure

MALDI-TOF mass spectrometry reveals that the protocol used to effect complete deuteration of the protein is effective; although much inhomogeneity is present, the protein mass is clearly increased. For a sample maintained in D_2O up until the measurement, the increase is consistent with the 198 exchangeable protons. For a sample allowed to incubate in normal H_2O for 12 hours before measurement, the mass increase was only about 35, with much less inhomogeneity in the peaks. This supports the reported results for NMR measurements, in which the core amide hydrogens are very resistant to solvent exchange.[12]

However, there are some difficulties with the approach. It was not always possible to recover immediately the characteristic blue copper color upon removal of the denaturant and reoxidation of the protein. In fact, it sometimes took additional attempts at reducing the protein and allowing it to incubate with copper to recover the color. The His109 mutant was the most severely affected, probably due to greater steric strain at the labeling site leading to misfolding, and was not recoverable. Although the unfolding of reduced azurin is reported to be reversible,[16] this is only the case when the native disulfide bond is not broken.[17] Dithionite may be too strong a reductant, in which case hydrogen over platinum would be a better alternative. However, samples exchanged by incubation in deuterated conditions for several weeks are not affected in this way, yet exhibit the same isotope effects.

Electrochemistry

Electrochemical measurements indicate little change in potential for both the ruthenium complex and the copper site, following exchange into a D_2O based buffer; the

small changes observed are certainly not large enough a change to explain the differences in ET rates for a system so close to the activationless limit.[18] The Ru(II/III) potential for the $Ru(bpy)_2(im)_2^{2+}$ model complex increased by 13 mV in D_2O Pi (from 966 mV to 979 mV vs. NHE). This would serve to increase the driving force in a deuterated buffer. The azurin Cu(I/II) potential (324 mV; Figures 4.2 and 4.3) showed very little change from the normal value (326 mV).[18]

Though it is small, the effect on the reduction potential of azurin is quite interesting. In other work, the azurin potential was about 10 mV higher in a deuterated buffer.[19] The apparent discrepancy probably results from inconsistent levels of deuterium incorporation in the protein matrix. When the measurements were repeated after incubation at elevated temperatures, the measured potential increased by nearly 10 mV, a result consistent with that reported by others. This indicates that in the short term, the ongoing slow exchange of protons is affecting the electronic nature of the active site.

Isotope effects on ET rates

The results are summarized in Table 4.1. The initial measurement of RuHis83azurin in D_2O-based phosphate buffer gives a rate (7.6×10^5 s^{-1}) that is slower than the same experiment in normal buffer (1.2×10^6 s^{-1}). This normal isotope effect is not what would be expected for increased coupling due to strengthened hydrogen bonds in the ET pathway. However, upon prolonged incubation the rate recovers somewhat (1.1×10^6 s^{-1}). Exchange of the deuterated buffer for one of normal composition gives an even faster rate (1.8×10^6 s^{-1}). Clearly, this is not a simple situation.

There are at least two isotope dependences at work, one the opposite of the other. The rate slows upon the deuteration of the readily exchanged proton sites and the solvent,

with $k_H/k_D \approx 1.6$. This may correspond to an increase in outer sphere reorganization energy as the hydrogen bonds in the solvent cage around the protein are strengthened upon deuteration. It may also indicate that strengthening of the hydrogen bonds to a ligand, such as cysteine, can lead to diminished electronic coupling to copper; however, as such hydrogen bonds are relatively inaccessible, this explanation appears unlikely.

As the extent of deuteration increases, the rate becomes faster. When the deuterated protein is then returned to a normal H_2O solution, an inverse isotope effect is observed ($k_H/k_D \approx 0.7$). This may indicate that the exchange of core protons leads to enhanced electronic coupling along the pathway through lowering of the zero-point potential for the hydrogen bonds, leading to an increase in their bond strength and rigidity. However, this rate enhancement may also indicate that a tightening of the copper active site is taking place, lowering the inner sphere reorganization energy. It is also possible that contraction of the protein has reduced the donor-acceptor distance under the direct distance model;[20] however, hydrogen bond contractions upon deuteration are typically less than 0.01 Å.[7] Even a cumulative effect would likely be too small to explain the result.

Comparisons to small molecule systems

Care should be taken not to confuse the nature of the isotope effects being discussed here with non-relevant systems. Most importantly, no hydrogen bond breakage/formation is suggested. As a result, isotope effects are going to be small in magnitude, unlike those seen in enzymatic centers.[21] Furthermore, while ET has been studied in a large number of small molecule systems,[22] most of the early examples involve bridges in which there is translocation of the hydrogen across the interface to compensate for the charge transfer of the electron.[23,24] Such systems give normal isotope effects ($k_H/k_D > 1$). Therefore, it is necessary

to examine model systems in which electron transfer is not coupled to proton movement. Similarly, short strong hydrogen bonds tend to weaken upon deuteration, eliminating other examples from consideration.[25] Although there are now some model compounds that incorporate peptide hydrogen bonds,[26,27] it is unfortunate that isotope effects are not reported for them.

Isotope effects in proteins

A recent report gives the deuterium isotope effect on intramolecular ET in azurin as determined from pulse radiolysis.[19] After simple solvent exchange, an inverse isotope effect is observed with $k_H/k_D \approx 0.7$. This is explained in terms of a slightly smaller thermal expansion in D_2O. However, this isotope effect is the opposite of what is seen in Ru-azurin, where simple solvent exchange leads to a slower rate in D_2O. It appears more likely that the solvent isotope effect behaves as expected: deuteration increases the outer sphere reorganization energy and slows the rate. This effect may be especially pronounced in Ru-azurin as the ruthenium label is highly solvent exposed. However, this effect could be offset by changes in the inner sphere reorganization energy upon tightening of the internal hydrogen bond framework.[28,29]

Any modifications at the copper site will be quite slow as the relevant hydrogen bonds are difficult to exchange. On the other hand, the hydrogen bonds near the disulfide radical at Cys3-Cys26 may be influenced more readily. While the reduction potential and associated thermodynamic parameters for the copper site are relatively easy to measure, that for the disulfide radical are much more difficult. Still, the different types and numbers of hydrogen bonds involved in the two systems offer the best explanation for the two sets of results.

Conclusion

Two different isotope effects are seen for intramolecular ET in ruthenium-*modified* azurin. A normal solvent kinetic isotope effect ($k_H/k_D \approx 1.6$) likely indicates an increase in outer sphere reorganization energy associated with stronger hydrogen bonds in the solvent cage around the system. An inverse kinetic isotope effect ($k_H/k_D \approx 0.7$) is seen when the fully deuterated protein is returned to a normal buffer. This may indicate increased electronic coupling between donor and acceptor due to stronger internal hydrogen bonds, but it is also possible that the inner sphere reorganization energy of the copper site is somewhat reduced through some sort of entatic mechanism.

References

(1) Onuchic, J. N.; Beratan, D. N.; Winkler, J. R.; Gray, H. B. *Annu. Rev. Biophys. Biomolec. Struct.* **1992**, *21*, 349-377.

(2) Beratan, D. N.; Onuchic, J. In *Protein Electron Transfer*; Bendall, D. S., Ed.; BIOS Scientific Publishers Ltd.: Oxford, 1996; pp 23-42.

(3) Beratan, D. N.; Onuchic, J. N.; Betts, J. N.; Bowler, B. E.; Gray, H. B. *J. Am. Chem. Soc.* **1990**, *112*, 7915-7921.

(4) Regan, J. J.; Dibilio, A. J.; Langen, R.; Skov, L. K.; Winkler, J. R.; Gray, H. B.; Onuchic, J. N. *Chem. Biol.* **1995**, *2*, 489-496.

(5) Langen, R. Thesis: "Electron Transfer in Proteins: Theory and Experiment," California Institute of Technology, 1995.

(6) Hvidt, A.; Nielsen, S. *Adv. Prot. Chem.* **1966**, *21*, 287-385.

(7) Sokolov, N. D.; Savel'ev, V. A. *Chemical Physics* **1994**, *181*, 305-317.

(8) Bowers, P. M.; Klevit, R. E. *J. Am. Chem. Soc.* **2000**, *122*, 1030-1033.

(9) Singh, T. R.; Wood, J. L. *J. Chem. Phys.* **1968**, *48*, 4567-4581.

(10) Singh, T. R.; Wood, J. L. *J. Chem. Phys.* **1969**, *50*, 3572-3576.

(11) Sokolov, N. D.; Vener, M. V.; Savel'ev, V. A. *J. Mol. Struct.* **1990**, *222*, 365-386.

(12) van de Kamp, M.; Canters, G. W.; Wijmenga, S. S.; Lommen, A.; Hilbers, C. W.; Nar, H.; Messerschmidt, A.; Huber, R. *Biochemistry* **1992**, *31*, 10194-10207.

(13) Chang, T. K.; Iverson, S. A.; Rodrigues, C. G.; Kiser, C. N.; Lew, A. Y. C.; Germanas, J. P.; Richards, J. H. *Proc. Natl. Acad. Sci.* **1991**, *88*, 1325-1329.

(14) Maniatis, T.; Fritsch, E. F.; Sambrook, J. *Molecular cloning: a laboratory manual*; Cold Spring Harbor Laboratory: Cold Spring Harbor, New York, 1982.

(15) Glasoe, P. K.; Long, F. A. *J. Chem. Soc. A* **1960**, 188-190.

(16) Leckner, J.; Wittung, P.; Bonander, N.; Karlsson, B. G.; Malmström, B. *J. Biol. Inorg. Chem.* **1997**, *2*, 368-371.

(17) Bonander, N.; Karlsson, B. G.; Vänngard, T. *Biochi. Biophs. Acta* **1995**, *1251*, 48-54.

(18) Di Bilio, A. J.; Hill, M. G.; Bonander, N.; Karlsson, B. G.; Villahermosa, R. M.; Malmstrom, B. G.; Winkler, J. R.; Gray, H. B. *J. Am. Chem. Soc.* **1997**, *119*, 9921-9922.

(19) Farver, O.; Zhang, J. D.; Chi, Q. J.; Pecht, I.; Ulstrup, J. *Proc. Natl. Acad. Sci. U. S. A.* **2001**, *98*, 4426-4430.

(20) Moser, C. C.; Page, C. C.; Chen, X.; Dutton, P. L. *J. Biol. Inorg. Chem.* **1997**, *2*, 393-398.

(21) Kohen, A.; Klinman, J. P. *Acc. Chem. Res.* **1998**, *31*, 397-404.

(22) Chang, C. J.; Brown, J. D. K.; Chang, M. C. Y.; Baker, E. A.; Nocera, D. G. In *Electron Transfer in Chemistry*; Balzani, V., Ed.; Wiley-VCH: Weinheim, Germany, 2001; Vol. 3, pp 409-461.

(23) de Rege, P. J. F.; Williams, S. A.; Therien, M. J. *Science* **1995**, *269*, 1409-1413.

(24) Turró, C.; Chang, C. K.; Leroi, G. E.; Cukier, R. I.; Nocera, D. *J. Am. Chem. Soc.* **1992**, *114*, 4013-4015.

(25) Osuka, A.; Yoneshima, R.; Okada, T.; Taniguchi, N.; Mataga, N. *Chem. Commun.* **1998**, 1567-1568.

(26) Williamson, D. A.; Bowler, B. E. *J. Am. Chem. Soc.* **1998**, *120*, 10902-10911.

(27) Tamiaki, H.; Maruyama, K. *Chem. Lett.* **1993**, 1499-1502.

(28) Malmström, B. *Eur. J. Biochem.* **1994**, *223*, 711-718.

(29) Randall, D. W.; Gamelin, D. R.; LaCroix, L. B.; Solomon, E. I. *J. Biol. Inorg. Chem.* **2000**, *5*, 16-19.

Table 4.1 ET rates in $Ru(bpy)_2(im)His83Azurin$ under varying deuteration conditions

Conditions	ET rate (s^{-1})	k_H/k_D relative to (1)	k_H/k_D relative to (4)
(1) Normal proton abundance	1.2×10^6	–	0.67
(2) Normal protein, deuterated buffer	7.6×10^5	1.6	–
(3) Deuterated protein and buffer	1.1×10^6	1.1	1.6
(4) Deuterated protein, normal buffer	1.8×10^6	0.67	–

Figure 4.1. Representative kinetics for intramolecular ET in $Ru(bpy)_2(im)His83azurin$ Data at 430 nm are fit to a single phase corresponding to the reduction of the Ru(III) intermediate. Data at 633 nm are fit to two phases: the fast bleach corresponding to the reduction of the copper site in azurin ($\approx 10^7\ s^{-1}$) and its subsequent reoxidation ($\approx 10^6\ s^{-1}$)

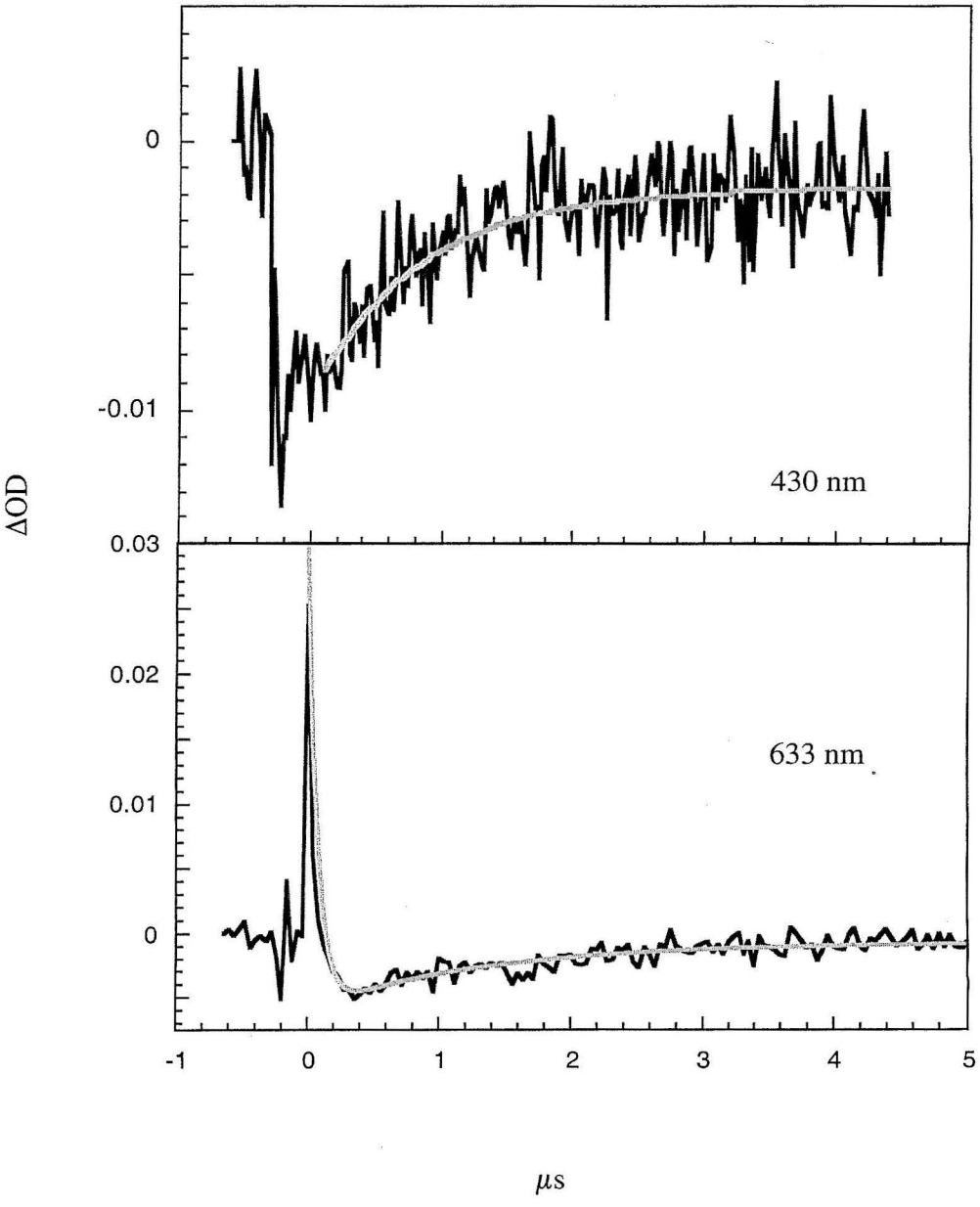
0
-0.01
430 nm
0.03
0.02
0.01
0
633 nm
-1
0
1
2
3
4
5
ΔOD
μs

Figure 4.2. Cyclic voltammetry for RuHis83Azurin

The wave shown is for the Cu^{2+}/Cu^{1+} couple at 25°C in D_2O Pi, $\mu = 0.1$, pD =7.1. The potential is about 116 mV vs. Ag/AgCl (324 mV vs. NHE, with calibration)

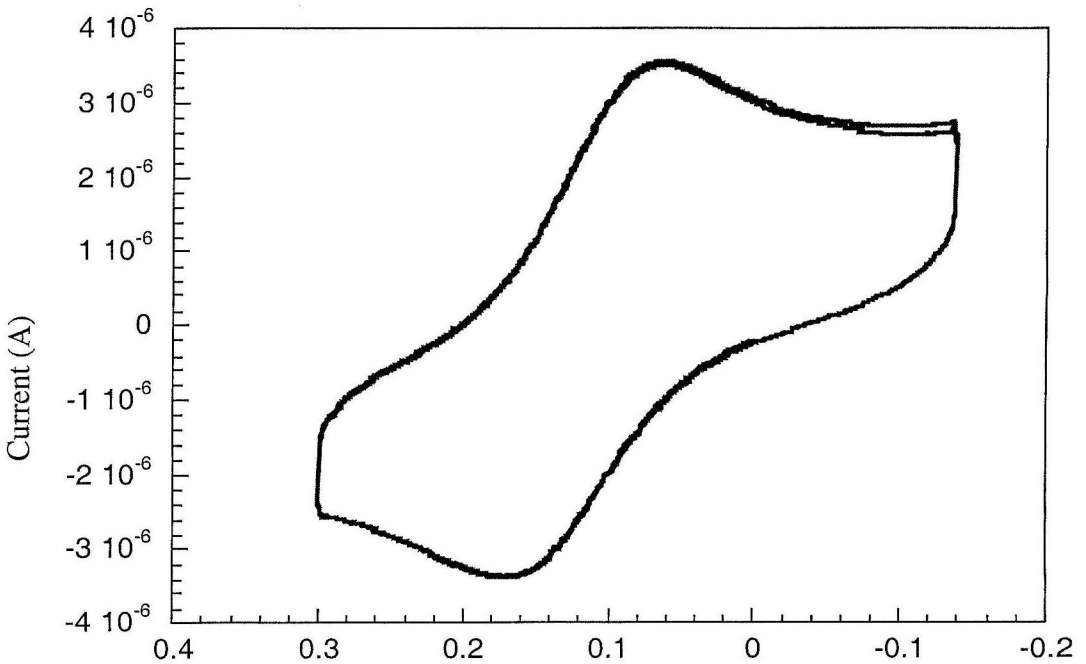
4 10-6
3 10-6
2 10-6
1 10-6
0
-1 10-6
-2 10-6
-3 10-6
-4 10-6
Current (A)
0.4
0.3
0.2
0.1
0
-0.1
-0.2
Potential vs. Ag/AgCl (V)

Figure 4.3. Temperature dependence of the reduction potential of azurin in D_2O buffer

The slope of the fit is proportional to $\Delta S°$, which in this case is – 63 J/mol•K.

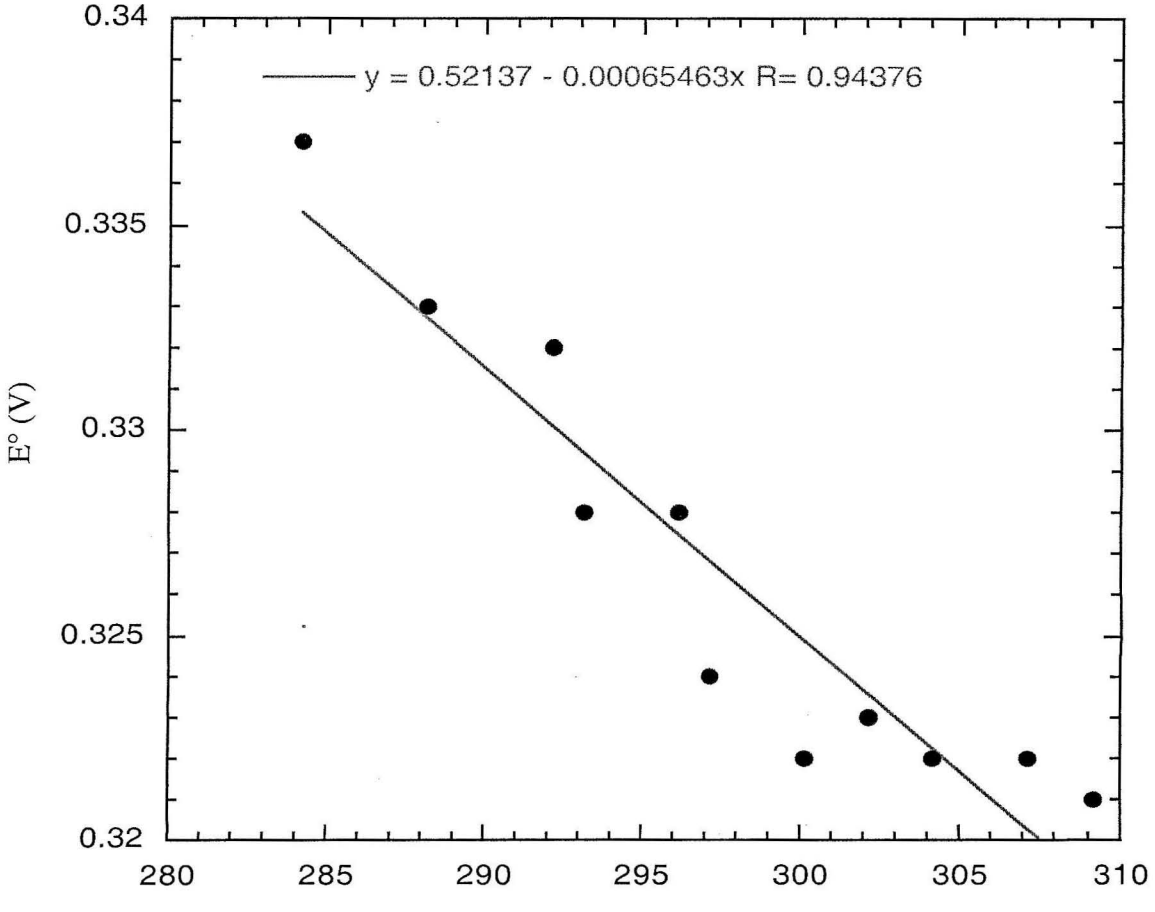
y = 0.52137 - 0.00065463x R= 0.94376
0.34
0.335
0.33
0.325
0.32
E° (V)
280
285
290
295
300
305
310
Temperature (K)

Figure 4.4. The structure of ruthenium modified azurin (wild type)

Selected solvent accessible surfaces are shown as dots. The copper site is well buried, the disulfide less so, and the ruthenium label is well exposed. Coordinates taken from PDB file 1BEX.

Appendix A

Expression and Purification of Cu_A

Background

The Cu_A subdomain from *T. thermophilus* was previously expressed in *E. coli* using the pET9a expression vector (Novagen) in the laboratory of Professor John H. Richards at Caltech. The *T. thermophilus* Cu_A domain was rendered a water-soluble protein by expressing only residues 34 through 168 of the subunit, which form the beta structure, and ignoring the transmembrane helical portions of the sequence. For purposes of ruthenium incorporation, this was further modified by the deletion of nine additional residues from the N-terminus, eliminating one of two surface histidines. Ruthenium modification at position 119 used the His117Q/E119H mutant of this "T9" construct. However, the residue numbering for this 125 amino acid protein is taken from the original numbering for the intact subunit.

Protein expression

Stocks of transformed cells containing the gene for H117Q/E119H Cu_A were stored at –80°C in 10% glycerol until needed. Scrapings were used to inoculate 50 mL cultures in TB containing 50 μg/mL kanamycin. These cultures were incubated for 8 hours at 37°C with vigorous shaking, then used to inoculate 2L of the same media and antibiotic in 6L flasks. Incubation of the larger culture continued for 4-6 hours, until an $OD_{600} \approx 1.0$ was attained. Induction by addition of IPTG to a final concentration of 0.4 mM was followed by an additional 6-hour incubation. The cells were harvested by centrifugation at 5000g for 5 min.

Lysis was carried out by suspending the cell pellet in 50mM Tris•HCl, pH = 8.0, at $1/10^{th}$ original volume. This suspension was then kept at –20°C overnight, or else until needed, then thawed. Triton was added to a final concentration of 0.1%, then the cells were

disrupted by sonication at the microtip limit in two cycles, each on for 30 s, then off for 30 s. In later preparations, this lysis protocol was replaced with one using BugBuster reagent with Benzonase (Novagen), supplementing the sample with Protease Inhibitor Cocktail for Bacterial Cell Extracts (Aldrich-Sigma). The cell debris was removed by centrifugation at 16,000g for 20 minutes and then the protein was promptly recovered from the lysate.

Protein purification

$CuSO_4$ from a 100 mM stock solution was added to the lysate to give 2-5mM Cu. The solution soon turned the characteristic purple color. For lysates in Tris•HCl, the flask containing the solution was warmed under running hot water to precipitate a mostly white material, which was removed by centrifugation. At times, the purple color would fade somewhat upon warming, but addition of more $CuSO_4$ would restore it. Then 50 mM NaOAc was added to the sample to give a pH ≈ 4.8 – 5.5. The H117Q/E119H mutant was notably less tolerant of lower pH, precipitating readily. As a result, this part of the protocol was later replaced with one using the BugBuster detergent formulation, which can be applied directly to an ion-exchange column.

The sample was loaded onto a 2.5 cm x 25 cm poured column containing CM–Sepharose Fast Flow cation exchange resin (Pharmacia) equilibrated in 20mM NaOAc, pH = 5.5. The column was washed with the same buffer at 2 ml/min for several hours, until purple protein began to elute from the bottom. However, there were two forms of the purple protein present, one binding more strongly to the column than the other. The column was drained down to the top of the resin, and then layers of the protein-bearing resin were removed with a spatula, divided into two fractions, and suspended in 20mM Tris•HCl w/ 1 M

NaCl, pH = 8.0. The resin was placed on a glass frit and the protein was washed off using this high-salt buffer.

As confirmed by mass spectrometry, the stronger binding material had a free N-terminus, whereas the weaker binding form was acetylated at the N-terminus. Such acetylation is a result of methionine removal during cytoplasmic processing. It was possible to resolve the two forms further using Mono Q anion exchange chromatography, where the positively charged N-terminus gives slightly weaker affinity for the column. Similarly, IMAC could be used, where the basic form of the free N-terminus provides slightly greater affinity for that column. For either case, adjusting the pH appropriately served to enhance the separation by influencing the extent of protonation of the free N-terminus.

None of the His variants bind very tightly to the CM-Sepharose column, as it is difficult to lower the pH substantially below the pI of the protein without precipitating protein. The three variants studied here exhibited binding affinities in the order: H117Q/E119H > wild type (H117) > H117Q/R148H. This order is consistent with the expected relative affinities of these proteins for the anionic resin. A similar effect was seen with MonoQ anion exchange chromatography, in the opposite order, and elution conditions were adjusted accordingly. The degree of separation for the acetylated and free N-terminus forms was dependent on the overall binding affinity of each variant. Thus, while there was some overlap between the two fractions for the wild-type protein (His117), there was marked separation for the H117Q/E119H mutant and extensive overlap for H117Q/R148H.

Each fraction was then desalted by repeated washings with 20 mM Tris•HCl, pH = 8 in an Amicon ultrafiltration device using a YM-10 membrane (Millipore). Then the protein was applied to a 5 mL HiTrap Q column (Pharmacia) equilibrated with the same buffer. The

column was washed with 15 mL of the buffer, and then the protein was eluted with 15 mL of the buffer containing 40 – 60 mM NaCl.

In preparations where a protease inhibitor was not used during lysis, there was often a small, tightly binding purple fraction left on the HiTrap Q column, eluting at 100 mM NaCl. Further FPLC purification of this material followed by characterization by mass spectrometry confirmed the presence of proteolytic fragments. The predominant of these was the fragment corresponding to cleavage after both Arg59 and Lys167.

Each fraction was further purified by FPLC, using a 10/10 Mono Q anion exchange column (Pharmacia). At first, buffer conditions were 20 mM Tris•HCl, pH 8.0 with a gradient of 0-200mM NaCl. Later it was found that using 10 mM Tris•HCl, pH 7.2 with a shallower gradient gave better resolution of the acetylated and free N-terminus. Reducing the protein with 1 mM DTT resulted in enhanced binding. Purified protein was exchanged into 25 mM HEPES w/ 30% glycerol, pH = 7, then stored at –20°C.

Appendix B

Expression and Metal Modification of Cytochrome *c*

Introduction

Surface modification of cytochrome *c* with photoactive ruthenium complexes has been used to study ET events in proteins.[1-3] Furthermore, ruthenium-modified cytochrome *c* can be used to initiate rapid ET events with other proteins such as cytochrome *c* oxidase[4] and cytochrome *c* peroxidase.[5,6] The ET rates and yields can be optimized by use of suitable metal complexes and ET quenching conditions.

The location of the surface label is also critical to the properties of such a system, especially when docking interactions with another protein are to be considered. Overexpression of cytochrome *c* in *E. coli*[7] provides a way to use site-directed mutagenesis to selectively place suitable residues for modification. The expression of a *c*-type cytochrome is complicated by the need to the enzymes required for ligation of the heme to the peptide backbone.[8]

Materials and Methods

General

The gene for yeast iso-1-cytocrome *c*, *cyc1*, was the gift of Dr. Grant Mauk (University of British Columbia)[7] and the cytochrome maturation gene cassette expressed on pEC86 was the gift of Dr. Linda Thöny-Meyer (ETH-Zürich).[8] Dr. Michele McGuirl was primarily responsible for bringing the two systems together by performing the initial manipulation of the cytochrome *c* gene into a different vector. In general, the same reagents and equipment were used for the expression and purification of cytochrome *c* as were used in the Cu_A and azurin work, except that 3,000 MW cutoff YM-membranes were used for ultrafiltration. Cytochrome *c* samples, both labeled and unlabeled, were kept covered in foil to prevent light-induced damage to the heme. Rhenium complexes were obtained from Dr. Angelo Di Bilio.[9]

Protein expression

After the cytochrome *c* gene was transferred to a pET21 vector, any necessary mutations were performed using the QuickChange kit (Stratagene), with PCR primers ordered from Gibco. The PCR products were checked on an agarose gel and then used to transform the XL-1 Blue strain of *E. coli*. Single colonies were taken from LB agar plates containing 50 μg/mL ampicillin and used to grow 3 mL cultures. The plasmid was isolated from the harvested cells using a Wizard Midiprep kit. Samples were assayed by UV-Vis spectroscopy for yield and purity ($R_{260/280} \approx 1.7$) before aliquots were sent for sequencing (Caltech's DNA Sequencing Core Facility).

A dual transformation by the heat shock method was used to insert the two plasmids, one containing the *cyc1* gene and the other the heme maturation gene cassette, into BL21(DEA3) *E. coli*. Transformants were grown on agar plates containing both 60 μg/mL ampicillin and 34 μg/mL chloramphenicol. Single colonies were picked and screened for protein expression in 3 mL cultures. Once a suitable colony was found, it was used to inoculate 50 mL TB or LB media containing both antibiotics. This was grown at 37 °C to an OD_{600} of 0.4 – 0.6, then used to inoculate 1 L of TB in a 4L flask, preferably after centrifugation to remove the original 50 mL of media and resuspension in fresh TB. This larger volume was grown to an OD_{600} exceeding 2.3, then induced with 1 mM IPTG. After an additional 4 – 6 hours, the cells were harvested by centrifugation to yield red pellets.

Osmotic shock gave a small yield of protein, so lysis with BugBuster in the presence of protease inhibitors was used instead. Following lysis, the cell debris was washed repeatedly with 20 mM sodium phosphate, pH = 7 (Buffer A), to remove more cytochrome *c*. The lysate was then loaded onto a 2.5 cm x 10 cm CM-Sepharose column equilibrated with Buffer A. The column was washed with 150 mL of Buffer A, then the same volume of Buffer A w/ 150 mM NaCl, and finally with sufficient Buffer A w/350 mM NaCl to elute the reduced Fe(II) form of the protein. Smaller amounts of the oxidized Fe(III) form were sometimes observed on the column and could be eluted with additional salt. Yields after this first column were 20 – 25 mg/L. Following oxidation with ferricyanide and exchange back into Buffer A, the protein was further purified using FPLC with a 16/10 Mono S cation exchange column (Pharmacia).

Metal modification

Ruthenium modification was done in a similar fashion as for Cu_A and azurin: the addition of a slight excess of $Ru(bpy)_2CO_3$ to a concentrated solution of the protein in 300 mM sodium bicarbonate. This was done in aliquots over a 48-hour period. Excess ruthenium was removed by ultrafiltration, and then solid imidazole was added to give a concentration of 500 mM. The sample was allowed to incubate in the dark for several days. Following removal of the excess imidazole by ultrafiltration and gel filtration, purification was accomplished using the 10/2 HR Chelating Sepharose FPLC column used for the azurin and Cu_A work. The second peak was typically the desired product, $Ru(bpy)_2$(im)His39cyt *c*, as determined by comparing the peaks at 316 nm and 410 nm in the electronic absorption spectrum and verified by mass spectrometry.

Rhenium modification was accomplished using $Re(CO)_3phen(H_2O)(CF_3CO_2)$, where phen is 1,10–phenanthroline. Cytochrome *c* in 250 μL 25 mM HEPES, pH = 7.4 was further diluted with 1 mL H_2O, and then kept at room temperature as aliquots of the Re complex in water were added over a 7–10 day period. The sample was concentrated and washed with 20 mM sodium phosphate using a Centricon–3 and then diluted with 500 μL 20 mM sodium phosphate w/ 750 mM NaCl, pH = 7 and allowed to sit for at least 24 hours. Any precipitate was removed by centrifugation and the sample purified by FPLC as for the ruthenium-labeled protein.

Kinetic measurements

Measurements of photoinduced ET in $Ru(bpy)_2$(im)His39cyt *c* were obtained using the same equipment and methods described in the earlier chapters. Observations were made at 426 and 550 nm. Samples were typically contained 10–15 μM protein in potassium

phosphate buffer, $\mu = 0.1$, pH = 7. For the reductive flash-quench approach, *p*-methoxy-*N,N*-dimethylaniline (MeODMA) was added to the sample at a concentration of 5 mM.

Results and Discussion

Protein expression

To give greater yields of protein and fewer difficulties in purification, yeast iso-1-cytochrome *c* was overexpressed in *E. coli*. As a result, there is incorporation of a normal lysine at position 72, not the trimethylysine that results from a post-translational modification in yeast.[7] In addition, there is a cysteine at position 102 in the native protein, but this residue was changed to threonine in the UBC construct and to serine at Caltech to prevent dimerization of the product protein. Efforts were made to follow the protocol accompanying the original *cyc1* construct;[7,10] however, this gave lower levels of expression in our situation.

The cytochrome *c* gene was taken from the original construct and moved into a pET21 vector along with a periplasmic leader sequence. This necessitated a Thr2Ala mutation to satisfy codon restrictions for insertion into the new plasmid, but this change was reversed in the final construct. The original gene also had an N–terminal methionine, which would ordinarily be removed in cytoplasmic processing. However, in the new periplasmic expression system it is not removed, so another mutation was made to delete this methionine.

In instances of high expression, cell pellets and even colonies on agar plates took on a reddish color, indicating the presence of cytochrome *c*. This suggested that the protein was being expressed into the periplasm, where the heme maturation occurs with this system. However, osmotic shock resulted in disappointedly low yields of protein in the extrudate, leaving behind bright red cell pellets. Two possible explanations were that the periplasmic leader sequence was not cleaved, leaving the protein tethered to the inner membrane, or simply that the high positive charge of cytochrome *c* (pI $\approx$ 10) gave it a high affinity for the polysaccharide wall of the cell. Indeed, washing the cell pellet with 0.5 M NaCl afforded a

substantial quantity of cytochrome *c*, so lysis was used to isolate the protein. Protease inhibitors are also recommended for this step. Following purification, mass spectrometry confirmed the presence of the desired cytochrome *c* (M^+ = 12,649)

Metal Modification:

Ruthenium modification of cyt *c* is straightforward. However, the isolation of the Ru(bpy)2(H2O)His39cyt *c* intermediate can be confusing with the 3 major peaks from the Chelating Sepharose column indicating the presence of 1, 2, or 3 equivalents of the ruthenium label. Incubation in imidazole eliminates the excess quantity of ruthenium, affording the desired 1:1 product. Mass spectrometry shows peaks at 12650 (unlabelled cyt *c* = 12,449), 13,061.8 (product without imidazole = 13, 063), and 13,128.8 (product = 13,131). This pattern of degradation is typical of measurements for labeled proteins, even when using electrospray mass spectrometry rather than MALDI-TOF.

Compared to ruthenium labeling, rhenium modification is much more difficult. An excess of rhenium complex leads to a product mixture with an average Re/Fe ratio of 10:1. Upon addition of high salt buffer, the protein precipitates. This is consistent with protein unfolding due to the destabilizing influence of the hydrophobic rhenium complexes in a solution of high ionic strength. Subsequent attempts employed a strategy similar to that used with ruthenium labeling, in which only slight excesses of metal complex are used, and the time scale of the incubation lengthened to overcome problems with poor reactivity. The yield was quite low, but the protein showed no signs of precipitation (M^+ = 13,098.2 observed vs. 13,100 predicted).

Kinetic measurements

The rate, 3 x 10^6 s^{-1}, for direct photoinduced intramolecular ET in $Ru(bpy)_2(im)His39cyt\ c$ agrees with that reported previously.[2] Using *p*-methoxy-*N,N*-dimethylaniline (MeODMA) as an exogenous quencher to generate Ru(I) does not seem to be very effective. The exogenous quenching reaction ($k_q \approx 6 \times 10^8\ M^{-1}s^{-1}$)[11] cannot compete with the intramolecular quenching reaction ($\approx 10^7\ s^{-1}$) and the resulting data only indicates the presence of the internal ET quenching. Doubling the concentration of MeODMA may help overcome this. However, after thousands of laser shots, reduction of the sample is apparent. This reduction does not occur in the dark. This suggests that the system is undergoing some exogenous quenching, as ET quenching with MeODMA is not completely reversible.[11]

Conclusions

The expression of cytochrome *c* in *E. coli* shows great promise for the rapid generation of cytochrome *c* mutants in high yield. Modification with photoactive metal ccomplexes continues to be a useful means to inject electrons into oxidized cytochrome *c*. In this case bimolecular reductive quenching may not be able to outpace intramolecular ET events; however, this may change if metal groups with different reduction potentials are used to slow the intramolecular ET rates. Rhenium complexes providing a higher driving force may be useful in this regard, if the ET rates are sufficiently inverted.

References

(1) Durham, B.; Pan, L. P.; Hall, J.; Millett, F. *Biochemistry* **1989**, *32*, 8659-8665.

(2) Wuttke, D. S.; Bjerrum, M. J.; Winkler, J. R.; Gray, H. B. *Science* **1992**, *256*, 1007-1008.

(3) Wuttke, D. S. Thesis: "Preparation, Characterization and Intramolecular Electron-Transfer Studies of Ruthenium-Modified Cytochromes *c*," California Institute of Technology, 1994.

(4) Pan, L. P.; Hibdon, S.; Liu, R.-Q.; Durham, B.; Millett, F. *Biochemistry* **1993**, *32*, 8492-8498.

(5) Hahm, S.; Durham, B.; Millett, F. *Biochemistry* **1992**, *31*, 3472-3477.

(6) Geren, L.; Hahm, S.; Durham, B.; Millett, F. *Biochemistry* **1991**, *30*, 9450-9457.

(7) Pollock, W. B. R.; Rosell, F.; Twitchett, M. B.; Dumont, M. E.; Mauk, A. G. *Biochemistry* **1998**, *37*, 6124-6131.

(8) Thöny-Meyer, L.; Künzler, P.; Hennecke, H. *Eur. J. Biochem.* **1996**, *235*, 754-761.

(9) Connick, W.; Di Bilio, A. J.; Hill, M. G.; Winkler, J. R.; Gray, H. B. *Inorg. Chem. Acta* **1995**, *240*, 169-173.

(10) Rosell, F. I. Thesis: "The Alkaline Conformational Transitions of Ferricytochrome *c*," University of British Columbia, 1999.

(11) Mines, G. A. Thesis: "Cytochrome *c*: Folding Triggered by Electron Transfer. Rates of Heme Oxidation and Reduction at High Driving Forces," California Institute of Technology, 1997.